Isotope effects of reactions in quantum solids initiated by IR + UV lasers: Quantum model simulations for Cl(2P3/2) + X 2(v) → XCl + X in X2 matrices (X = H, D)

ARTICLE *in* THE JOURNAL OF PHYSICAL CHEMISTRY A · SEPTEMBER 2010

Impact Factor: 2.69 · DOI: 10.1021/jp102809p · Source: PubMed

3 AUTHORS, INCLUDING:

M. V. Korolkov

National Academy of Sciences of Belarus

66 PUBLICATIONS **710** CITATIONS

SEE PROFILE

Isotope Effects of Reactions in Quantum Solids Initiated by IR + UV Lasers: Quantum Model Simulations for $Cl(^2P_{3/2}) + X_2(\nu) \rightarrow XCl + X$ in X_2 matrices (X = H, D)†

M. V. Korolkov,*,‡,§ J. Manz,‡ and A. Schild‡

Institut für Chemie und Biochemie, Freie Universität Berlin, Takustrasse 3, 14195 Berlin, Germany, and Institute of Physics, National Academy of Sciences of Belarus, Minsk, Belarus

Received: March 29, 2010; Revised Manuscript Received: May 14, 2010

Six isotope effects (i)−(vi) are discovered for the reactions $Cl + H_2(\nu) \rightarrow HCl + H$ in solid para-H_2 (1) versus $Cl + D_2(\nu) \rightarrow DCl + D$ in ortho-D_2 (2), by means of quantum reaction dynamics simulations, within the frame of our simple model (*J. Phys. Chem. A* **2009**, *113*, 7630.). Experimentally, the reactions may be initiated for $\nu = 0$ and $\nu \geq 1$, by means of "UV only" photodissociation of the matrix-isolated precursor, Cl_2, or by "IR + UV" coirradiation (Kettwich, S. C.; Raston, P. L.; Anderson, D. T. *J. Phys. Chem. A* **2009**, *113*, 7621.), respectively. Specifically, (i) various shape and Feshbach reaction resonances correlate with vibrational thresholds of reactants and products, due to the near-thermoneutrality and low barrier of the system. The energetic density of resonances increases as the square root of mass, from $M_X = M_H$ to M_D. (ii) The state selective reaction (1), $\nu = 1$, is supported by a shape resonance, whereas this type of resonance is absent in (2), $\nu = 1$. As a consequence, time-resolved measurements should monitor different three-step versus direct error-function type evolutions of the formation of the products. (iii) The effective barrier is lower for reaction 1, $\nu = 0$, enhancing the tunneling rate, as compared to that for reaction 2, $\nu = 0$. (iv) For reference, the reaction probabilities P versus total energy E_{tot} in the gas exhibit sharp resonance peaks or zigzag behaviors of the reaction probability P versus total energy, near the levels of resonances (Persky, A.; Baer, M. *J. Chem. Phys*. **1974**, *60*, 133.). These features tend to be washed out and broadened for reaction 1, and even more so for reaction 2. For comparison, they disappear for reactions in classical solids. (v) The slopes of P versus E_{tot} below the potential barrier increase more steeply for reaction 1, $\nu = 0$, than for reaction 2, $\nu = 0$. This enhances the tunneling rate of the heavier isotopomer, reaction 2, $\nu = 0$, compared to that for reaction 1. (vi) For a given value of the UV frequency, the translational energy E_{trans} increases with mass M_X. Again, this effect supports tunneling of the heavier isotopomer. The isotope effects (i)−(iii), (iv)−(v), and (vi) may be classified as energetic, translational amplitude, and kinematic, respectively. Specifically, the effects (iv)−(v) are due to a systematic decrease of the amplitudes of translational motions of the reactant molecules, from quasi infinite in the gas via still rather large values of para-$H_2(\nu)$ and smaller values for ortho-$D_2(\nu)$ to very small values in classical solids. These isotope effects are special phenomena in quantum solids, which do not occur, neither in the gas phase nor in classical solids. Quantitative predictions, e.g., for the effects of increasing UV frequency on the ratio of reactions probabilities for the UV only versus IR + UV experiments, must account for the interplay of various isotope effects, e.g., (vi) combined with the antagonistic effects (iii) versus (iv) and (v).

I. Introduction

Recent experiments by the groups of Anderson[1–3] and Momose[4] and co-workers have opened the field of photoinduced elementary reactions in quantum solids at low temperatures, typically below 10 K. These studies provide important double extensions of previous experimental and theoretical investigations, from nonreactive to reactive molecular processes in quantum solids, and from reactions in rare gas matrices to quantum solids, see for example refs 5 and 6 and 7–12, respectively.

A prominent example is the reaction

$$Cl(^2P_{3/2}) + H_2(\nu) \xrightarrow{\text{para-}H_2} HCl + H \qquad (1)$$

in solid para-H_2, which has been investigated by means of two experiments that prepare the reactant $H_2(\nu)$ in different vibrational states, $\nu = 0$ and $\nu = 1$:[3] The first one ($\nu = 0$), referred to as "only UV", employs near resonant ultraviolet (UV) irradiation (wavelength $\lambda = 350$ nm corresponding to photon energy $\hbar\omega = 3.782$ eV) to photodissociate a matrix-isolated Cl_2 precursor molecule in the C $^1\Pi_u$ state. This generates the atomic reactant $Cl(^2P_{3/2})$, which may react with a para-$H_2(\nu = 0)$ molecule of the matrix, albeit with rather low reaction probability, $P_{\nu=0} \approx 0.006$. The second experiment ($\nu = 1$), referred to as "IR + UV", combines the UV excitation with infrared (IR) coirradiation, which induces vibrational preexcitation of the molecular reactant, $H_2(\nu = 1)$. As a consequence, the reaction probability is enhanced by a factor ∼25 to $P_{\nu=1} \approx 0.15$.

We have carried out quantum model simulations of the reaction 1 in solid para-H_2[13] that account for important features of the "only UV" versus "IR + UV" experiments.[3] Essentially, we could show that the experimental results are consequences of energetic and dynamical effects, which are different in the quantum solid from those for reaction 1 in the gas phase; see, for example, refs 14–23. Some important details of the model will be described in chapter II.

† Part of the "Reinhard Schinke Festschrift".

* Corresponding author. E-mail: korolkovmv@yahoo.com.
‡ Freie Universität Berlin.
§ National Academy of Sciences of Belarus.

10.1021/jp102809p
Published on Web 06/10/2010

The purpose of this paper is to extend the theoretical investigation of reaction 1 to

$$Cl(^2P_{3/2}) + D_2(\nu) \xrightarrow{\text{ortho-}D_2} DCl + D \qquad (2)$$

in solid ortho-D_2. Comparison of the results should provide the first prediction of vibrational state selective isotope effects of elementary reactions in quantum solids. For reference, comparative investigations of kinetic isotope effects of reactions 1 and 2 in the gas phase are documented in refs 14–17; for complementary examples of isotope effects of elementary reactions in the gas phase, see also refs 24–36. We focus on specific isotope effects that should stimulate corresponding experiments. For this purpose, we shall employ the common notation

$$Cl(^2P_{3/2}) + X_2(\nu) \xrightarrow{\text{solid } X_2} XCl + X \qquad (3)$$

where X = H or D and solid X_2 denotes the quantum solids with isotopomers para-H_2 or ortho-D_2. Important properties of these quantum solids have been reviewed in ref 37; see also refs 38 and 39.

The model and techniques are adapted from refs 13 and 40. They are summarized in chapter II, for self-consistent presentation of the isotope effects. The model is based on several assumptions;[13] it serves as a reference for extensions. Chapter III presents the methods for discovering and analyzing resonances in reactions 3. The results of the quantum model simulations for reaction 2 are presented and compared with those of reaction 1, in chapter IV, together with discussions of trends that allow us to deduce working hypotheses for extended models and experiments. The conclusions are in chapter V.

II. Model and Techniques

The model for the quantum simulations of reactions 3 contains several items that are significant for the purpose of this paper, i.e., predictions of isotope effects. These are summarized below; for additional details, see refs 13 and 40. Essentially, it assumes that, initially, the system consists of the quantum solid, with the central X_2 molecule substituted by a Cl_2 molecule in the electronic and vibrational ground state $X^1\Sigma_g^+$, $\nu = 0$. Effects of geometric relaxations of the matrix that surrounds the central guest molecule (cf. ref 41) are neglected. Furthermore, for reference we assume that the reactions 3 are between the photodissociated chlorine atom $Cl(^2P_{3/2})$ and a neighboring $X_2(\nu)$ molecule of the quantum crystal, located at nearest neighbor distance R_{0,X_2}. The values of R_{0,X_2} depend on the isotopomer X_2, specifically

$$R_{0,H_2} = 7.16a_0 \qquad \text{and} \qquad R_{0,D_2} = 6.82a_0 \qquad (4)$$

for para-H_2 and ortho-D_2, respectively.[37] This rather small variation of R_{0,X_2} is considered, however, as irrelevant for isotope effects of reactions 3.

Next it is assumed that the reactions 3 proceed in three steps. First, the "only UV" and "IR + UV" experiments prepare the molecular reactants $X_2(\nu)$ in vibrational states $\nu = 0$ or 1, respectively. In chapter IV, we shall also investigate hypothetical scenarios of molecular reactants $D_2(\nu = 2$ or 3), corresponding to vibrational overtone excitations by IR + UV experiment with larger IR frequencies. Accordingly, the reactants $Cl(^2P_{3/2}) + X_2(\nu)$ are represented approximately in terms of translational and vibrational wave functions,[13]

$$\Psi_{Cl+X_2(\nu)}(x,y;t_0) = \Psi_{trans,par}(x,t_0) \times \Psi_{X_2(\nu)}(y) \qquad (5)$$

Here and below, we adapt the general notation of ref 13, i.e., the wave functions are written with the variables in brackets, and subscripts for the parameters (par), to be specified below; analogous notations are used for the corresponding probability densities, or probabilities, etc. Specifically, the vibrational wave functions $\Psi_{X_2(\nu)}(y)$ are modeled as Morse oscillator wave functions, depending on the internuclear distance y, as in the gas phase. The corresponding parameters, i.e., the equilibrium bond length $y_{e,X_2} = 1.402\ a_0$, the well depth $D_{X_2} = 4.748$ eV, and the Morse parameter $\beta_{X_2} = 1.028\ a_0^{-1}$, are the same for both isotopomers, $X_2 = H_2$ or D_2; their values are adapted from the gas phase[42] (similar to data in ref 15), neglecting weak perturbations of the vibrational levels in the quantum solids.[13] The corresponding vibrational energies

$$E_{X_2(\nu)} = -D_{X_2} + (\nu + 0.5)\hbar\omega_{X_2} - \frac{((\nu + 0.5)\hbar\omega_{X_2})^2}{4D_{X_2}} \qquad \nu = 0, 1, ..., \nu_{max,X_2} \qquad (6)$$

decrease with increasing masses $M_H = 1.0079$ and $M_D = 2.0136$ u and the corresponding reduced masses $\mu_{X_2} = M_X/2$ of the isotopomers, due to the relation

$$\mu_{X_2}\omega_{X_2}^{\ 2} = 2D_{X_2}\beta_{X_2}^{\ 2} \qquad (7)$$

for the vibrational frequencies ω_{X_2}. For small vibrational quantum numbers, the vibrational motions are nearly harmonic, such that (6) and (7) imply the (approximate) energetic isotope effect

$$\frac{E_{D_2(\nu)} + D_{D_2}}{E_{H_2(\nu)} + D_{H_2}} \approx \sqrt{\frac{M_H}{M_D}} \qquad (8)$$

Moreover, the numbers of vibrational levels

$$\nu_{max,X_2} = \left[\frac{2D_{X_2}}{\hbar\omega_{X_2}} - \frac{1}{2}\right] \qquad (9)$$

and the corresponding level densities increase with mass,

$$\frac{\nu_{max,D_2}/D_{D_2}}{\nu_{max,H_2}/D_{H_2}} \approx \sqrt{\frac{M_D}{M_H}} \qquad (10)$$

The brackets $[u]$ in eq 9 denote the largest integer smaller than u, such that $\nu_{max,H_2} = 16$ and $\nu_{max,D_2} = 24$.

Analogous expressions hold for the energy levels of the products of reactions 3,

$$E_{XCl(\nu)} = -D_{XCl} + (\nu + 0.5)\hbar\omega_{XCl} - \frac{((\nu + 0.5)\hbar\omega_{XCl})^2}{4D_{XCl}} \qquad \nu = 0, 1, ..., \nu_{max,XCl} \quad (11)$$

$$\mu_{XCl}\omega_{XCl}{}^2 = 2D_{XCl}\beta_{XCl}{}^2 \quad (12)$$

where $\mu_{XCl} = M_X M_{Cl}/(M_X + M_{Cl})$, hence

$$\frac{E_{DCl(\nu)} + D_{DCl}}{E_{HCl(\nu)} + D_{HCl}} \approx \sqrt{\frac{M_H}{M_D}} \quad (13)$$

as well as

$$\nu_{max,XCl} = \left[\frac{2D_{XCl}}{\hbar\omega_{XCl}} - \frac{1}{2}\right] \quad (14)$$

$$\frac{\nu_{max,DCl}/D_{DCl}}{\nu_{max,HCl}/D_{HCl}} \approx \sqrt{\frac{M_D}{M_H}} \quad (15)$$

The Morse parameters $y_{e,XCl} = 2.406\ a_0$, $D_{XCl} = 4.629$ eV, and $\beta_{XCl} = 0.989\ a_0{}^{-1}$ are also adapted from refs 13 and 42, again assuming that any perturbations by the quantum solid are negligible. Accordingly, $\nu_{max,HCl} = 24$ and $\nu_{max,DCl} = 34$.

The translational motions of the reactants $X_2(\nu)$ are described in the frame of the extended Einstein model of ref 39. It assumes that all other molecules are frozen at their equilibrium positions. Gratifyingly, this Einstein model accounts for the isotope effects of structural and energetic properties of the quantum solids, such as the different nearest neighbor distances (4), the different sublimation energies,[37] and—most importantly for the present application—the different widths ΔR_{X_2} of the center-of-mass distributions of the reactant molecules X_2. Specifically, at the given low temperatures, the $X_2(\nu)$ molecules carry out nearly harmonic motions in the corresponding Einstein cells. Accordingly, the wave functions of the reactants X_2 are well approximated by Gaussians centered at R_{0,X_2}, with rather broad width parameters ΔR_{X_2}. These decrease with mass as

$$\frac{\Delta R_{D_2}}{\Delta R_{H_2}} \approx \sqrt{\frac{M_H}{M_D}} \quad (16)$$

see ref 39. Specifically,

$$\Delta R_{H_2} = 1.09 a_0 \qquad \text{and} \qquad \Delta R_{D_2} = 0.81 a_0 \quad (17)$$

The corresponding densities have full widths at half-maximum (fwhm) 2.57 and 1.93 a_0, respectively.[39] Likewise, our model assumes that the Cl_2 ($X^1\Sigma_g^+, \nu = 0$) precursor molecules are embedded in corresponding Einstein cells of the X_2 quantum solids, with much smaller width parameters[13]

$$\Delta R_{Cl_2} \approx \left(\frac{M_X}{M_{Cl}}\right)^{1/2} \Delta R_{X_2} \quad (18)$$

The second step of our model[13] describes the preparation of the atomic reactant

$$Cl_2(X^1\Sigma_g^+, \nu = 0) \xrightarrow{\hbar\omega} Cl_2(C^1\Pi_u) \rightarrow 2Cl(^2P_{3/2}) \quad (19)$$

by Franck−Condon type UV photoexcitation of the matrix-isolated Cl_2 ($X^1\Sigma_g^+, \nu = 0$) precursor molecule to the $C^1\Pi_u$ state, with photon energy $\hbar\omega$, followed by photodissociation. The corresponding energy of photoexcitation is shared equally between the two chlorine atoms; for reference, in the gas phase, the difference

$$\Delta E(\omega) = \hbar\omega - (2E_{Cl(^2P_{3/2})} - E_{Cl_2(\nu=0)}) \quad (20)$$

between the UV photon energy minus the dissociation energy of Cl_2 in the electronic ground state would be converted into equal shares of pure translational energy of the two chlorine atoms. In contrast, for reactions 3 in solid quantum crystals, we anticipate (by extrapolation of previous investigations of photodissociation of diatomic molecules in rare gas matrices[43–45]) that, in principle, this second step (19) could induce an avalanche of processes that involve an increasing number of degrees of freedom, from initial bond stretch via first interactions with the neighboring molecules until energy transfer from the two chlorine atoms to possibly many molecules of the quantum solid. For reference, let us consider first the limiting case of an initial period that lasts as long as the interaction of the $Cl(^2P_{3/2})$ atoms with the molecules of the surrounding quantum solids are still negligible, analogous to the initial stretch of the Cl_2 bond length during photodissociation in the gas phase; effects of energy transfer to the matrix will be considered in chapter IV. The end of this period, i.e., the onset of significant interactions, defines our initial time t_0 for the approach of the atomic and molecular reactants $Cl(^2P_{3/2}) + X_2(\nu)$, with decreasing distance x between $Cl(^2P_{3/2})$ and the center of mass of $X_2(\nu)$. For convenience, we set $t_0 = 0$. Photodissociation in the quantum solid during this period ($t < t_0$) is somewhat analogous to the photodissociation of diatomic molecules in weakly bound clusters.[46–48] The corresponding translational wave function is well approximated by a Gaussian[13]

$$\Psi_{trans,k_{Cl+X_2}(\omega),\Delta x_{Cl+H_2}}(x;t_0) = N_{Cl+X_2} \exp\left[-\frac{1}{2}\left(\frac{x - x_0}{\Delta x_{Cl+H_2}}\right)^2 + i\hbar k_{Cl+X_2}(\omega)(x - x_0)\right] \quad (21)$$

Here x_0 is the mean distance at time t_0; $\hbar k_{Cl+X_2}(\omega)$ is the relative translational momentum of the reactants with total mass $M = M_{Cl} + 2M_X$ and reduced mass $\mu_{Cl+X_2} = 2M_X M_{Cl}/M$, depending on the frequency ω of the UV laser, and Δx_{Cl+H_2} is the widths parameter. Due to kinematic constraints of the photodissociation in the matrix,[13] the related relative translational energy of the reactants along coordinate x in the quantum solid is restricted to a small fraction M_X/M of the energy $\Delta E(\omega)$ of the two dissociated chlorine atoms in the gas phase,[13]

$$E_{trans}^X(\omega) = \frac{(\hbar k_{Cl+X_2}(\omega))^2}{2\mu_{Cl+X_2}} = \frac{M_X}{M}\Delta E(\omega) \quad (22)$$

This imposes a kinematic isotope effect

$$\frac{E^{\mathrm{D}}_{\mathrm{trans}}(\omega)}{E^{\mathrm{H}}_{\mathrm{trans}}(\omega)} = \frac{M_{\mathrm{D}}}{M_{\mathrm{H}}} \tag{23}$$

i.e., for the same UV laser frequency, the relative translational energy of the reactants Cl + D_2 is about twice as large as for Cl + H_2. Analogous kinematic isotope effects apply to reactions in the gas and in classical solids.

The width parameter of the translational wave function (21), $\Delta x_{\mathrm{Cl+X_2}}(\tau,\Delta R_{\mathrm{Cl_2}},\Delta R_{\mathrm{X_2}})$, depends on three other width parameters: $\Delta R_{\mathrm{X_2}}$ for the translational motion of X_2 in its Einstein cell; cf. eq 17; $\Delta R_{\mathrm{Cl_2}}$ for the corresponding translational motion of the Cl_2 molecule, cf. eq 18; and, for reference, the width parameter $\Delta q_{\mathrm{Cl}}(\tau)$ of the wavepacket that would describe the photodissociated chlorine atom in the gas, at time t_0, depending on the duration τ of the laser pulse. The lower limit of $\Delta q_{\mathrm{Cl}}(\tau)$ can be estimated from the width parameter $\Delta y_{\mathrm{Cl_2},\nu=0} = 0.25\ a_0$ of the vibrational wavepacket of Cl_2 ($X^1\Sigma_g^+,\nu = 0$), for the scenario of ultrashort (delta-pulse) Franck−Condon excitation. The upper limit is infinity, for the case of continuous wave (cw) excitation. Specifically,

$$\Delta x_{\mathrm{Cl+X_2}} = \left(\frac{C_{\mathrm{Cl}}{}^2}{\Delta R_{\mathrm{X_2}}{}^2} + \frac{C_{\mathrm{X_2}}{}^2}{\Delta R_{\mathrm{Cl_2}}{}^2 + \Delta q_{\mathrm{Cl}}(\tau)^2}\right)^{-1/2} \tag{24}$$

with mass coefficients $C_{\mathrm{Cl}} = M_{\mathrm{Cl}}/M$ and $C_{\mathrm{X_2}} = 2M_{\mathrm{X}}/M = 1 - C_{\mathrm{Cl}}$.[13] Consideration of the second term on the rhs of eq 24, together with the limits for $\Delta q_{\mathrm{Cl}}(\tau)$, yields modest variations of $\Delta x(\tau,\Delta R_{\mathrm{Cl_2}},\Delta R_{\mathrm{X_2}})$, approximately between the rather narrow limits

$$\left(\frac{C_{\mathrm{Cl}}{}^2}{\Delta R_{\mathrm{X_2}}{}^2} + \frac{C_{\mathrm{X_2}}{}^2}{\Delta R_{\mathrm{Cl_2}}{}^2}\right)^{-1/2} < \Delta x_{\mathrm{Cl+X_2}}(\tau,\Delta R_{\mathrm{Cl_2}},\Delta R_{\mathrm{X_2}})^2 < \frac{\Delta R_{\mathrm{X_2}}}{C_{\mathrm{Cl}}} \tag{25}$$

Using eqs 17 and 18 and the masses $M_{\mathrm{H}} = 1.0079$ u, $M_{\mathrm{D}} = 2.0136$ u, and $M_{\mathrm{Cl}} = 34.968852$ u, we obtain

$$\begin{aligned} &1.06a_0 \lesssim \Delta x_{\mathrm{Cl+H_2}} \lesssim 1.15a_0 \text{ for reaction 1 and} \\ &0.78a_0 \lesssim \Delta x_{\mathrm{Cl+D_2}} \lesssim 0.90a_0 \text{ for reaction 2} \end{aligned} \tag{26}$$

In ref 13, a slightly larger upper limit, i.e., 1.27 a_0, has been derived for reaction 1, due to a slightly larger estimate of $\Delta R_{\mathrm{H_2}} = 1.21\ a_0$, compared to 1.09 a_0, eq 17. Below we shall employ these upper limits (26), which correspond to laser pulses with durations $\tau \geq 50$ fs.[13] Obviously, $C_{\mathrm{Cl}} \approx 1 \gg C_{\mathrm{X_2}}$; i.e., the width $\Delta x(\tau,\Delta R_{\mathrm{Cl_2}},\Delta_{\mathrm{X_2}})$ is dominated by the first term on the right-hand side (rhs) of eq 24, which accounts for the translational width of $X_2(\nu)$ in its Einstein cell, thus

$$\Delta x_{\mathrm{Cl+X_2}}(\tau,\Delta R_{\mathrm{Cl_2}},\Delta R_{\mathrm{X_2}}) \approx \Delta R_{\mathrm{X_2}} \tag{27}$$

see Table 2 in ref 13. The approximation (27) implies that the isotope effect, eq 16, holds approximately also for the relative translational motions of the reactants,

$$\frac{\Delta x_{\mathrm{Cl+D_2}}(\tau,\Delta R_{\mathrm{Cl_2}},\Delta R_{\mathrm{D_2}})}{\Delta x_{\mathrm{Cl+H_2}}(\tau,\Delta R_{\mathrm{Cl_2}},\Delta R_{\mathrm{H_2}})} \approx \frac{\Delta R_{\mathrm{D_2}}}{\Delta R_{\mathrm{H_2}}} \approx \sqrt{\frac{M_{\mathrm{H}}}{M_{\mathrm{D}}}} \tag{28}$$

As a consequence, the translational wavepacket for Cl + D_2 has a narrower spatial width than for Cl + H_2. Due to the uncertainty relation, the spatial widths parameter $\Delta x_{\mathrm{Cl+X_2}}$ implies the corresponding widths of the translational momenta

$$\hbar\Delta k_{\mathrm{Cl+X_2}} = \frac{\hbar}{\sqrt{2}\Delta x_{\mathrm{Cl+X_2}}} \tag{29}$$

and of the translational energies

$$\Delta E^{\mathrm{X}}_{\mathrm{trans}} = \sqrt{\frac{E^{\mathrm{X}}_{\mathrm{trans}}}{\mu_{\mathrm{Cl+X_2}}}}\frac{\hbar}{\Delta x_{\mathrm{Cl+X_2}}} \tag{30}$$

For a given UV laser frequency, eqs 23 and 28 then imply the isotope effect

$$\frac{\Delta E^{\mathrm{D}}_{\mathrm{trans}}}{\Delta E^{\mathrm{H}}_{\mathrm{trans}}} \approx \sqrt{\frac{M_{\mathrm{D}}}{M_{\mathrm{H}}}} \tag{31}$$

i.e., Cl + D_2 has a larger width of the translational energy than Cl + H_2.

For convenience, the translational wave function $\Psi_{\mathrm{trans},k_{\mathrm{Cl+X_2}}(\omega),\Delta x_{\mathrm{Cl+X_2}}}(x,t_0)$, eq 21, is renormalized using $N_{\mathrm{Cl+X_2}} = (1/\pi\Delta x^2)^{1/4}$, irrespective of the laser intensity. Moreover, we combine steps (1) and (2) such that the initial wave functions of the translational and vibrational motions of the reactants Cl($^2P_{3/2}$) + $X_2(\nu)$ in the quantum solid are

$$\Psi_{\mathrm{Cl+X_2}(\nu),k_{\mathrm{Cl+X_2}}(\omega),\Delta x_{\mathrm{Cl+X_2}}}(x,y;t_0=0) = \Psi_{\mathrm{trans},k_{\mathrm{Cl+X_2}}(\omega),\Delta x_{\mathrm{Cl+X_2}}}(x;t_0=0)\Psi_{\mathrm{X_2}(\nu)}(y) \tag{32}$$

at the end t_0 of (1) and (2), which marks the beginning of step (3).

Reactions 3 describe the reaction of the molecular and atomic reactants. For reference, we assume again that the quantum solid is frozen during this elementary process. To simplify the model even further, we adapt some important properties of the potential energy surface (PES) for the reactions 3 in the gas phase; in particular, it favors a collinear approach.[15,19,20] Accordingly, we employ a collinear model for reactions 3, with coordinates x and y for the distance between the Cl atom and the center of mass of the two atoms X_2, and for the bond lengths of the diatomic fragment X_2. For convenience, we use $\Psi_{\mathrm{Cl+X_2}}(x,y;t_0 = 0)$, eq 32, as initial wave functions. Their time evolutions are then evaluated as solutions of the time-dependent Schrödinger equation

$$\mathrm{i}\hbar\frac{\mathrm{d}}{\mathrm{d}t}\Psi_{\mathrm{Cl+X_2}(\nu),k_{\mathrm{Cl+X_2}}(\omega),\Delta x_{\mathrm{Cl+X_2}}}(x,y,t) = H\Psi_{\mathrm{Cl+X_2}(\nu),k_{\mathrm{Cl+X_2}}(\omega),\Delta x_{\mathrm{Cl+X_2}}}(x,y,t) \tag{33}$$

with Hamilton operator

$$H = T_{x,y} + V(x,y) \tag{34}$$

using the numerical techniques described in ref 13. The potential energy surface is modeled as so-called London−Eyring−Polanyi−Sato LEPS PES, fitted to the ab initio PES of Capecchi and Werner.[19] The LEPS parameters include the Morse parameters of the reactants and products, vide infra, as well as the Sato parameters $S_{X_2} = 0.170$ and $S_{XCl} = 0.183$[13,49–51] for adjusting the height and location of the potential barrier E_b. For a contour plot of V, see Figure 2a in ref 13. As a consequence of E_b, the LEPS PES does not support any bound states of the ClX_2 system. Again, any weak perturbations of the intramolecular interactions of the reactive triatomic systems $X + Cl_2$ by the environment are neglected. The intermolecular interactions of the system with the different quantum solids are taken into account implicitly, cf. eqs 21, 24, 26, and 32.

The kinetic energy operator is

$$T_{x,y} = -\frac{\hbar^2}{2\mu_{Cl+X_2}}\frac{\partial^2}{\partial x^2} - \frac{\hbar^2}{2\mu_{X_2}}\frac{\partial^2}{\partial y^2} \tag{35}$$

The mean total energy of the wavepacket is

$$E_{tot,Cl+X_2(\nu)} = E_{X_2(\nu)} - E_{X_2(0)} + E^X_{trans} \tag{36}$$

The formation of the products is monitored by the time-dependent reaction probability. It is calculated as the integral of the density

$$\rho_{Cl+X_2(\nu),k(\omega),\Delta x}(x,y,t) = |\Psi_{Cl+X_2(\nu),k(\omega),\Delta x}(x,y,t)|^2 \tag{37}$$

in the asymptotic domain, $y > y_b$,

$$P_{XCl+X\leftarrow Cl+X_2(\nu),k(\omega),\Delta x}(t) = \int_0^\infty dx \int_{y_b}^\infty dy\, \rho_{Cl+X_2(\nu),k(\omega),\Delta x}(x,y,t) \tag{38}$$

In the application below, we use $y_b = 3\ a_0$; the results are not sensitive to the choice of y_b, within resonable limits. Finally, the net reaction probability is calculated as the long time limit

$$P_{XCl+X\leftarrow Cl+X_2(\nu),k(\omega),\Delta x} = P_{XCl+X\leftarrow Cl+X_2(\nu),k(\omega),\Delta x}(t \rightarrow \infty) \tag{39}$$

Further details are in ref 13.

III. Reaction Resonances: From Gas to Quantum Solids

For the subsequent discussion of reaction resonances, analogous analyses of resonances of the $F + H_2$ reaction in the gas,[52] see also refs 53 and 54 that suggest employing hyperspherical coordinates, also called "Delves" coordinates,[55,56]

$$r = \sqrt{x_m^{\,2} + y^2} \tag{40}$$

$$\phi = \arctan(y/x_m) \tag{41}$$

where x_m is the mass-weighted (m) coordinate

$$x_m = \sqrt{\frac{\mu_{Cl,X_2}}{\mu_{X_2}}}\, x \tag{42}$$

The hyperspherical radius r describes the mean distance between the three atoms of the collinear system Cl−X−X. For example, r is small for short distances in the interaction domain close to the potential barrier. In contrast, r approaches infinity for the configurations of the reactants as well as for the products. The hyperspherical angle ϕ accounts for the motion of the central atom X betwen the outer ones. For example, for small values of r, the angle ϕ describes motions from configuration Cl·XX to ClX·X. In contrast, for large values of r, the angle ϕ describes vibrations of X_2 as well as XCl. Moreover, since motions along r involve all atoms including the heavy Cl, wheras motion along ϕ involves exclusively the light atom X, it is convenient to employ a separation of r and ϕ that may be called the second Born−Oppenheimer separation, analogous to the here called first BO separation of the coordinates Q and q describing the motions of the nuclei and electrons, respectively;[57] see also refs 27, 29, 31, and 58–72. The well-known first BO separation of Q and q suggests the first Born−Oppenheimer approximation (BOA1): here the wave functions for electrons and nuclei are approximately written as products of electronic times nuclear wave functions $\Psi_{el,nu}(q,Q) \approx \Psi_{el}(q;Q) \times \Psi_{el,nu}(Q)$, with quantum numbers "el" and "nu", respectively. Solving the electronic Schrödinger equation for fixed nuclear coordinates Q, this ansatz yields the electronic adiabatic potential energy surfaces $V_{el}(Q)$ for nuclear motions, depending parametrically on fixed values of Q. For large values of Q, the $V_{el}(Q)$ approach the electronic eigenenergies of the corresponding separated molecular fragments, which may be considered as reactants or products.

By analogy with BOA1, the second BO separation suggests the second BOA (BOA2). Here, one makes the ansatz[60]

$$\Psi_{\nu_\phi,\nu_r}(\phi,r) \approx \Psi_{\nu_\phi}(\phi;r) \times \Psi_{\nu_\phi,\nu_r}(r) \tag{43}$$

with quantum numbers $\nu_\phi = 0, 1, 2, ...$ and $\nu_r = 0, 1, 2, ...$ for motions along ϕ and r, respectively. Solving the hyperspherical angular equation for fixed value of r, this ansatz yields the wave functions $\Psi_{\nu_\phi}(\phi;r)$ as well as the adiabatic potential curves $V_{\nu_\phi}(r)$ for motions along the hyperspherical radius r.[27,29,31,59–67,69,70,72] The $V_{\nu_\phi}(r)$ are ordered with increasing energies $V_0(r) < V_1(r) < V_2(r) < ...$ for $\nu_\phi = 0, 1, 2, ...$ Asymptotically, for $r \rightarrow \infty$, the potential curves $V_{\nu_\phi}(r)$, approach the vibrational levels of the reactants $E_{X_2}(\nu)$ and products $E_{XCl}(\nu')$; see eqs 6 and 11. Accordingly, these levels may be renamed E_{ν_ϕ}, in energetic order. In the other limit $r \rightarrow 0$, the $V_{\nu_\phi}(r)$ are always repulsive because it costs energy to compress the system Cl−X−X to configurations with very small values of r. Between these limits, $r \rightarrow \infty$ and $r \rightarrow 0$, the $V_{\nu_\phi}(r)$ may exhibit hyperspherical radial potential minima with or without neighboring local barriers. These potential minima support the BOA2 eigenstates, eq 43 with wave functions Ψ_{ν_ϕ,ν_r} and energies E_{ν_ϕ,ν_r} for radial motions in the V_{ν_ϕ} versus r. In general, the E_{ν_ϕ,ν_r} are approximations to levels of bound states if they are below the levels of the vibrational ground states of the reactants as well as of the products. As discussed above, the LEPS PES does not, however, support any bound states. Instead, it supports quasi-bound states that have higher BOA2 energies $E_{\nu_\phi\nu_r}$. For reference, these are called resonances, for reactions 1 and 2 in the gas phase.[14–17] In refs 13 and 40 we have shown that some phenomena of resonances are also manifest in reaction 1 in solid p-H_2. It is a

challenge to search for similar phenomena in reaction 2 in solid ortho-D_2, and to discover isotope effects related to resonances in (3). For this purpose, let us summarize various properties of the reaction dynamics related to resonances.

If a BOA2 resonance has energy $E_{\nu_\phi \nu_r} > E_{\nu_\phi}$, it means that $\Psi_{\nu_\phi,\nu_r}(r)$ is trapped in a minimum of $V_{\nu_\phi}(r)$ with neighboring potential barrier. Then it may decay by tunnelling; this type of resonance is called shape resonance.[31,73] Otherwise it can decay only by transitions to lower $V_{\nu'_\phi}(r)$ with $\nu'_\phi < \nu_\phi$; then it is called Feshbach resonance. Bound states or resonances with levels labeled $E_{\nu_\phi,\nu_r=0}$ are called hyperspherical modes;[60–62,64,66,67,70,72,74] their BOA2 wave functions (43) extend along periodic orbits[75–78] (see also refs 79 and 80) that resemble arcs with approximately constant values of r, and ν_ϕ nodes along ϕ but without any nodes along r. Of course, the exact solutions include couplings between the BOA2 states labeled ν_ϕ and ν_r, and these introduce level shifts as well as distortions of the BOA2 wave functions (43). Nevertheless, often one of them is dominant, and then the quantum numbers ν_ϕ and ν_r may be assigned to the exact wave functions as well.[63] Isotopic substitutions may also cause distortions of the shapes of the wave functions (43), e.g., from hyperspherical modes to hyperellipsoidal ones.[81]

Since each vibrational state of the reactants and products $E_{\nu_\phi} = E_{X_2(\nu)}$ or $E_{XCl(\nu')}$ correlates with a specific BOA2 potential $V_{\nu_\phi}(r)$ that may support just one hyperspherical state with quantum numbers $\nu_\phi,\nu_r = 0$, provided $V_\phi(r)$ has a suitable potential minimum, it follows that each vibrational state E_{ν_ϕ} correlates with either one or zero hyperspherical resonance, with levels close to $E_{\nu_\phi,\nu_r=0}$. As an empirical result, the selected set of resonances that correlate with the vibrational $E_{\nu_\phi} = E_{X_2(\nu)}$ of the reactants, may form a systematic series of resonances, e.g., similar to the levels of a Morse oscillator, albeit with Morse parameters that are different from those of the rectants or products; see, e.g., ref 60. Likewise, there is a complementary systematic series of resonances that correlate with the product levels $E_{\nu'_\phi} = E_{XCl(\nu')}$. If one has already discovered some of the members of these series, then one can extrapolate to predict the energies of additional resonances, which are still missing. These may then either be verified, for example, by propagations of wave functions as discussed below, or not. If the missing resonances do not exist, then one may conclude that the correlating potential $V_{\nu_\phi}(r)$ is repulsive; i.e., it does not possess any significant potential minimum that might support a BOA2 resonance (43).

The formation and decay of resonances may have several effects on time-independent[54,82–85] as well as time-dependent quantum reaction dynamics.[40,86] For reference, in the gas phase, ideal unimolecular resonance decay proceeds exponentially[54,62,64,66,70,72,74,83–85] with decay time τ_{ν_ϕ,ν_r} depending on the quantum numbers, and corresponding energetic widths

$$\Gamma_{\nu_\phi,\nu_r} = \frac{\hbar}{\tau_{\nu_\phi,\nu_r}} \tag{44}$$

Time-dependent quantum simulations of bimolecular reaction dynamics[13,40] with representative wave functions $\Psi_{Cl+X_2(\nu),k,\Delta x}(x,y,t)$, starting from the reactants $Cl + X_2(\nu)$, eq 43, show different mechanisms, depending on whether the total energy (36) is off or on resonance. If $E_{tot,Cl+X_2(\nu)}$ is far away from any resonance energy E_{ν_ϕ,ν_r}, then the corresponding nonresonant (nrs) wave function runs to the interaction region where it separates into partial waves representing elastic and inelastic scattering (S) back to the reactants, or direct reaction (R) to the products. The corresponding time-dependent nonresonant (nrs) reaction probabilities (38) increase with universal error function type behavior,[40]

$$P_{nrs,XCl+X\leftarrow Cl+X_2(\nu),k,\Delta x}(t) \approx P_{nrs,XCl+X\leftarrow Cl+X_2(\nu),k,\Delta x}\,\mathrm{erf}\left(\frac{t - t_h}{t_{nrs}}\right) \tag{45}$$

where $P_{nrs,XCl+X\leftarrow Cl+X_2(\nu),k,\Delta x}$ denotes the nonresonant net reaction probability, t_h (half time) is the time when $P_{nrs,XCl+X\leftarrow Cl+X_2(\nu),k,\Delta x}(t=t_h) = 1/2P_{nrs,XCl+X\leftarrow Cl+X_2(\nu),k,\Delta x}$, and t_{nrs} specifies the nonresonant rise time. In contrast, if $E_{tot,Cl+H_2(\nu)} \approx E_{\nu_\phi,\nu_r}$, the wave function consists of two components, one for the nonresonant (nrs) background, with rather rapid direct reactivity similar to that in eq 45, and the other one for slower indirect elastic and inelastic scattering (S) or reactivity (R) via the resonance (res),

$$\Psi_{Cl+X_2(\nu),k,\Delta x}(x,y,t) = \Psi_{nrs,Cl+X_2(\nu),k,\Delta x}(x,y,t) + \Psi_{res,Cl+X_2(\nu),k,\Delta x}(x,y,t) \tag{46}$$

Both components run synchronously from the reactant configuration (32) to the interaction region. Here, the nonresonant component separates into two partial waves for elastic and inelastic scattering (S), and for direct reaction (R), as described above; cf. eq 45. In contrast, the resonant component forms the resonance wave function, which is located in the interaction domain, with quantum numbers ν_ϕ and ν_r. Subsequently, it decays exponentially toward the reactants as well as to the products, in accord with unimolecular resonance decay and the corresponding decay time τ_{ν_ϕ,ν_r}. Broad empirical evidence shows that hyperspherical resonances have rather long lifetimes $\tau_{\nu_\phi,\nu_r=0}$, compared to the lifetimes of other (e.g., local) resonances or the time for direct, nonresonant reaction.[62,64,66,70,72,74] The reactivity of the resonant component $\Psi_{res,Cl+X_2(\nu),k,\Delta x}(x,y,t)$ is thus mediated by a rather long-lived hyperspherical resonance; hence it is called indirect. The unimolecular energetic widths, eq 44, are modified in time-dependent bimolecular reactions, however, due to the finite widths in space, Δx, momentum, eq 29, and energy, eq 30, of the initial wave function (32) (see section IV). For extended discussions of relations between uni- and bimolecular reactivity mediated by a resonance, see, e.g., refs 61 and 69.

The superposition (46) of the two nonresonant and resonant components with fast direct and rather slow indirect reactivities causes product formation in three sequential steps:[40] Initially, the fast, nonresonant component causes error function type increase of the time-dependent reaction probability (39), analogous to eq 45. Next, there may be a short period of transition from dominantly nonresonant to resonant increases of the reaction probability, with rich phenomena, e.g., oscillatory reactivity due to interferences of the two components. Finally, the slower reactivity due to formation and exponential decay of the resonance provides the corresponding additional, rather late, growth of the reaction probability, according to

$$P_{XCl+X\leftarrow Cl+X_2(\nu),k,\Delta x}(t) = P_{nrs,XCl+X\leftarrow Cl+X_2(\nu),k,\Delta x} + P_{res,XCl+X\leftarrow Cl+X_2(\nu),k,\Delta x}\left(1 - \exp\left(-\frac{t - t_{\nu_\phi,\nu_r}}{\tau_{\nu_\phi,\nu_r}}\right)\right) \tag{47}$$

where $P_{\mathrm{nrs,XCl+X\leftarrow Cl+X_2}(\nu),k,\Delta x}$ and $P_{\mathrm{res,XCl+X\leftarrow Cl+X_2}(\nu),k,\Delta x}$ are nonresonant and resonant contributions to the net reaction probability, τ_{ν_ϕ,ν_r} is the same as the decay time for unimolecular resonances, and t_{ν_ϕ,ν_r} is the resonance delay time. All parameters in eq 47 depend on the quantum numbers of the resonance.

At sufficiently long times, when the time-dependent reaction probability proceeds according to eq 47, the nonresonant component of the wave function, eq 46, has already penetrated completely into the domains of the products or reactants. The only component that still survives in the interaction domain is the resonant one. Its shape may then be discovered and analyzed using a late snapshot of its densitity. The robustness of the shape is confirmed by good agreement with snapshots that are taken at even later times. Often the resonant wave function resembles the ideal hyperspherical BOA2 wave function, eq 43, with quantum numbers $\nu_\phi,\nu_r = 0$. In this case one can determine the quantum number ν_ϕ by counting the number ν_ϕ of nodal lines perpendicular to the arc along the angle ϕ. Moreover, in ideal cases, the quantum number $\nu_r = 0$ is verified if the density of the resonance wave function shows a single maximum along r, i.e., zero nodal lines perpendicular to r. Realistic cases may show a single dominant maximum along r, which may be accompanied by small neighboring ones, due to the coupling of the dominant BOA2 wave function (43) with quantum numbers $\nu_\phi,\nu_r = 0$, with others that have larger quantum numbers ν_r. Turning the table, the emergence of a resonance wave function with hyperspherical shape, in the interaction domain, at rather late times provides evidence for the existence of the resonance with corresponding quantum numbers $\nu_\phi,\nu_r = 0$ and energy close to the BOA2 value $E_{\nu_\phi,\nu_r=0}$.

The energetic width (44), which is associated with unimolecuar resonance decay in the gas phase, serves as a reference. For reactions 3 in quantum solids, we define the corresponding resonance energy domain $\Delta E_{\mathrm{XCl+X\leftarrow Cl+X_2}(\nu),k,\Delta x,\nu_\phi,\nu_r}$. It depends on the initial vibrational level (6), the translational energy (22), the spatial width Δx, and the quantum numbers ν_ϕ and ν_r of the given resonance. The resonance energy domain is the range of total energies (36) that yield the three-step-formation of products,[40] as discussed above. In contrast, total energies causing error function type formation of products (45) are off-resonant; i.e., they are out of the resonance energy domain. In practice, the resonance energy domain is determined by analyzing the resonant versus nonresonant product formations of many wave functions (46), which have the same parameters, except for systematic variations of the momentum $\hbar k$ and the corresponding translational and total energies, eqs 22 and 36, respectively.

Another signature of resonances are significant deviations of the reaction probabilities (39) versus total energy (36) from the general trends in off-resonant domains, close to the levels of the resonances, i.e., close to $E_{\nu_\phi,\nu_r=0}$. These deviations may appear as resonance peaks (or dips or zigzag features) that are superimposed on otherwise rather smooth plots of the reaction probabilities versus total energy. This phenomenon may be rationalized as a consequence of the superposition (46) of the two nonresonant and resonant components, which support different reaction mechanisms, including not only the different rapid direct versus slow indirect reactivities, respectively (vide infra), but also different branching ratios for the partial waves that are scattered back to the reactants, or that react to the products. Rather sharp resonance peaks for reactions 1 and 2 in the gas phase have been documented already in refs 15–17 using methods of time-independent scattering theory, but without analyses in terms of hyperspherical modes, and still without classification as Feshbach ($E_{\nu_\phi,\nu_r} < E_{\nu_\phi}$) or shape ($E_{\nu_\phi,\nu_r} > E_{\nu_\phi}$) resonances. In ref 13, we discovered related rather smooth or partially washed-out resonance peaks, also for reaction 1 in solid para-H_2. This motivates the subsequent systematic analysis of isotope effects for resonance phenomena in reactions 3 in quantum solids, centering attention on similarities with, and deviations from, the results in the gas phase. For example, in the gas phase, resonances are characterized by the total energy.[82] As a consequence, the energies of resonance peaks coincide as long as the reactants react with the same total = translational plus vibrational energy (36), irrespective of the vibrational level of the reactants. Will the resonance energy domains of reactions 3 be the same for different vibrational pre-excitations, and will they also overlap in the quantum solids? Our investigation will employ all the criteria for resonances that have been outlined above, including time-dependent reaction probabilities with signatures of three-step reactivity, snapshots of the densities of resonance wave functions with hyperspherical shapes that are taken during the late third step, and peaks or zigzag features in the reaction probabilities versus total energy.

IV. Results and Discussion

Section II, which is based on the model of ref 13, suggests various types of isotope effects of reactions 1 versus 2 in the quantum solids, para-H_2 and ortho-D_2, respectively. The subsequent analysis starts with some phenomena that are similar to isotope effects for the corresponding reactions in the gas phase. Subsequently, we shall consider special isotope effects in quantum solids.

First, our model uses the same series of vibrational levels (6) and (11) of the reactant and product molecules X_2 and XCl for reactions 3 in the quantum solids as for the gas phase. This approximation is a consequence of the rather weak interactions of these molecules with the surrounding quantum solids, at and beyond the rather large nearest neighbor distances, eq 4. The lowest levels of these series are illustrated Figures 1 and 2 (bottom panels) for X = D and H, respectively. Also shown in Figures 1 and 2 (top panels) are the corresponding vibrational thresholds

$$\Delta E^{\mathrm{XS}}_{\nu\nu'} = E_{\mathrm{X_2}(\nu')} - E_{\mathrm{X_2}(\nu)}(\mathrm{S}) \tag{48}$$

and

$$\Delta E^{\mathrm{XR}}_{\nu\nu'} = E_{\mathrm{XCl}(\nu')} - E_{\mathrm{X_2}(\nu)}(\mathrm{R}) \tag{49}$$

for inelastic scattering (S)

$$\mathrm{Cl} + \mathrm{X_2}(\nu) \xrightarrow{\text{solid } \mathrm{X_2}} \mathrm{Cl} + \mathrm{X_2}(\nu') \tag{50}$$

or vibrational state (ν)-to-state (ν') reactions (R)

$$\mathrm{Cl} + \mathrm{X_2}(\nu) \xrightarrow{\text{solid } \mathrm{X_2}} \mathrm{X} + \mathrm{XCl}(\nu') \tag{51}$$

see also Tables 1 (S) and 2 (R), respectively.

The resulting approximate isotope effects for the low vibrational levels of the reactants, eq 8, and for the products, eq 13, as well as for the numbers of all vibrational levels and

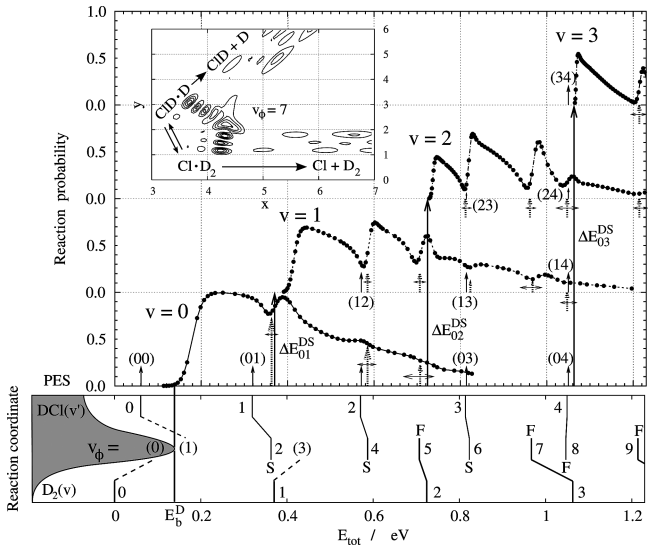

Figure 1. Reaction probabilities (eq 39) of the model Cl + ortho-$D_2(v) \rightarrow$ DCl + D reaction in ortho-D_2 (top panel) versus total energy $E_{tot} = \Delta E^{DS}_{0v} + E^{D}_{trans}$ (eq 36), for $v = 0$, 1, 2, 3 and width parameter $\Delta x = 4.25\ a_0$, eq 48. The vibrational thresholds for the levels of the reactants (labeled ΔE^{DS}_{0v}, eq 49) and the products ($\Delta E^{DR}_{vv'}$ with shorthand notation (vv'), eq 46, are indicated by means of long thick versus short thin vertical arrows, respectively. Also shown are the resonance energy domains (short horizontal arrows) as well as the corresponding mean resonance energies (dashed vertical arrows), which are close to the second Born−Oppenheimer BOA2 levels $E_{v_\phi,v_r=0}$. The corresponding hyperpherical quantum numbers v_ϕ are assigned in the bottom panel; quantum numbers (v_ϕ) in brackets indicate missing resonances. The resonance energies correlate with the vibrational levels of the reactants and products, as illustrated by thick and thin continuous correlation lines, respectively. Missing resonances are indicated by dashed correlation lines. The inset in the top panel shows a snapshot of the density of the wave function (37) after its nonresonant component has left toward the domains of reactants and products, whereas the resonant components survives in the interaction domain. The coordinates x and y are for the distance from the Cl($^2P_{3/2}$) atoms to the center of mass of ortho-D_2 and for the D_2 bond length, repsectively. The resonance resembles the hyperspherical BOA2 wave function, eq 43, revealing the dominant quantum number $v_\phi = 7$, in accord with the assignments of v_ϕ in the bottom panel. Shape and Feshbach resonances with central resonance energies above or below the correlating vibrational thresholds are labeled S or F, respectively. Also shown is a sketch of the LEPS potential energy surface PES (adapted from ref 13 where it has been fitted to the ab initio results of ref 19) versus the reaction coordinate, from the reactants Cl + D_2 via the barrier E_b to the products DCl + D (inset with gray domain on the left-hand side of the bottom panel).

the corresponding level densities, eqs 10 and 15, have several consequences.

(i) As explained in section II, in second Born−Oppenheimer approximation BOA2, the vibrational levels of the reactants and products correlate with effective potentials $V_{v_\phi}(r)$, which may support hyperspherical shape (S) or Feshbach (F) resonances with energies close to $E_{v_\phi,v_r=0}$, above or below the corresponding vibrational levels, respectively. Figures 1 and 2 (bottom panels) show the corresponding correlation diagrams for these vibrational levels and for the resonance energies of reactions 2 and 1, respectively. The assignments of the corresponding hyperspherical quantum number v_ϕ, as well as the resonance energy domains have been determined using the methods outlined in section III. Exemplarily, the inset in the top panel of Figure 1 shows the density of the resonance wave function, which is generated as the resonant component of the wave function starting from reactants Cl + $D_2(v = 2)$ at $E_{trans} = 0.24$ eV; cf. eqs 32 and 46. It survives in the interaction domain, after the partial waves of the nonresonant component have penetrated into the domains of the reactants and products. Obviously, the resonance wave function extends along an arc, from configuration Cl·D_2 to ClD·D. The arc has approximately constant hyperspherical radius r and arc length $r\phi$, where ϕ is the hyperspherical angle. There are seven nodal lines pependicular to the arc; this determines the hyperspherical angular quantum number $v_\phi = 7$. The dominant lobes along the hyperpherical radius r confirm the quantum number $v_r = 0$; marginal additional side lobes along r indicate that the resonance consists of the dominant BOA2 wave function $\Psi_{v_\phi=7,v_r=0}(\phi,r)$ (43) with small couplings to other BOA2 wave functions that have neighboring quantum numbers.

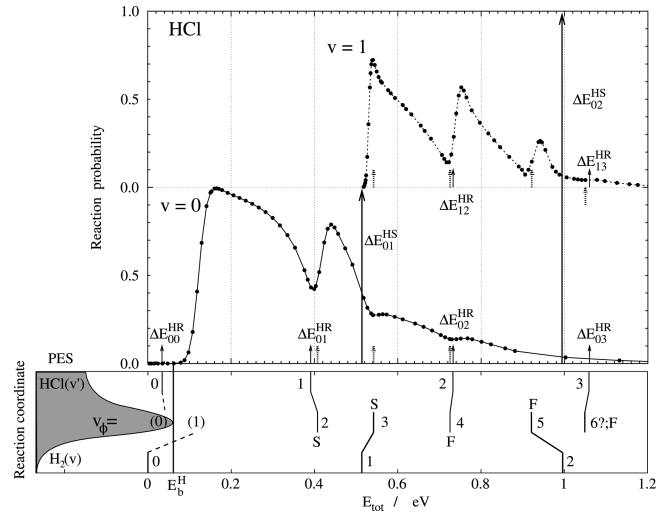

Figure 2. Same as Figure 1, but for the Cl + para-$H_2(v) \rightarrow$ HCl + H reaction in para-H_2, for $v = 0$, 1 and $\Delta x = 4.25\ a_0$ (adapted from ref 13). The resonance energy domains are not shown. The question of the expected Feshbach resonance 6?;F is discussed in the text.

TABLE 1: Vibrational Thresholds for Inelastic Scattering[a]

v	v'	$\Delta E^{DS}_{vv'}$/eV	$\Delta E^{HS}_{vv'}$/eV
0	1	0.370	0.514
0	2	0.724	0.994
0	3	1.063	1.447
1	2	0.354	0.482
1	3	0.693	0.934

[a] Eqs 48 and 50.

As anticipated in section II, the correlation diagrams in Figures 1 and 2 (bottom panels) show two series of resonances. One of them correlates with the vibrational levels of the reactants, the other one correlates with the product levels. The level spacings are similar to those of different Morse oscillators, with systematic trends that allow us to predict the levels of missing resonances; these are indicated by dashed correlation lines with hyperpherical numbers (v_ϕ) in brackets. In zero-order approximation, all correlation lines are approximately iso-energetic. This can be rationalized as consequences of the near-thermoneutrality of reactions 3, and of the rather small barrier E_b; see the insets with the schematic profiles of the LEPS PES along the reaction paths, in Figures 1 and 2 (bottom panels). As a consequence, for the lowest values of v_ϕ, the effective potentials $V_{v_\phi}(r)$ are repulsive; this means that they cannot support any resonances, in accord with the missing resonances in Figures 1 and 2. The correlation

diagrams suggest, furthermore, that for increasing values of ν_ϕ, the $V_{\nu_\phi}(r)$ form minima with increasing well depths. According to our BOA2 analysis, the type of resonances with increasing values of ν_ϕ switches from shape to Feshbach resonances, with energies above and below the correlated vibrational thresholds, respectively. This explains the systematic small but significant deviations of the correlations lines from the iso-energetic reference.

The near iso-energicity of the levels of the resonances and the vibrational levels of the reactants and products implies an isotope effect; i.e., the numbers and the corresponding energetic densities of the resonances increase with mass,

$$\frac{\text{no. of resonances for Cl + } D_2(\nu)/D_{DCl}}{\text{no. of resonances for Cl + } H_2(\nu)/D_{HCl}} \approx \sqrt{\frac{M_D}{M_H}} \tag{52}$$

in accord with eqs 10 and 15. The isotope effect (52) is obvious from Figures 1 and 2, which show a much higher energetic density of resonances for reaction 2 compared with those for reaction 1.

(ii) An important special case of the general trends of item (i) is the resonance labeled $\nu_\phi = 3$. It correlates with the first excited reactant state, $X_2(\nu = 1)$. The lower vibrational energy of $D_2(\nu = 1)$ compared to that for $H_2(\nu = 1)$ (cf. eq 8) implies that the energetically lower potential $V_{\nu_\phi=3}(r)$ is still repulsive for the Cl + $D_2(\nu = 1)$ reaction (cf. the missing resonance $\nu_\phi = 3$ in Figure 1), whereas it already forms a potential minimum that can support a Feshbach resonance labeled $\nu_\phi = 3$ for the Cl + $H_2(\nu = 1)$ reaction. In ref 13, we have already argued that the reactivity of the "IR + UV" experiment for the Cl + $H_2(\nu = 1)$ reaction in solid para-H_2 profits from this resonance (but without any systematic discussion in terms of, e.g., the quantum number $\nu_\phi = 3$, and without classification as Feshbach resonance), compared to the reactivity of the "UV only" experiment for the Cl + $H_2(\nu = 0)$ reaction, as measured by the group of Anderson.[3] The present analysis now allows us to predict another isotope effect; i.e., the "IR + UV" experiment for the Cl + $H_2(\nu = 1)$ versus Cl + $D_2(\nu = 1)$ reactions in solid para-H_2 versus ortho-D_2 profit/do *not* profit from a resonance. For example, if the experiment of ref 3 could be extended to a time-reolved pump−probe experiment, then one should observe different time evolutions of the formations of the products, i.e., direct fast formation of DCl, eq 45, in contrast with the slower, partially indirect three-step-formation of HCl, eqs 46 and 47.

(iii) The vibrational ground states of the reactants $D_2(\nu = 0)$ and products $DCl(\nu' = 0)$ have lower zero point energies than $H_2(\nu = 0)$ and $HCl(\nu' = 0)$, respectively. As a consequence, the effective potential barrier $\Delta E_{b,X_2} = E_b - E_{X_2(\nu = 0)}$ is larger for $X_2 = D_2$ than for H_2,

$$E_b^D = 0.139\text{eV} \qquad \Delta E_b^H = 0.061\text{eV} \tag{53}$$

See the bottom panels of Figures 1 and 2, respectively. This isotope effect suggests that tunneling through the barrier is more demanding for reaction 2 than for (1). This conjecture is supported by the fact that the mass associated with tunneling is heavier for reaction 2 than for reaction 1. By analogy with the reactions in the gas phase,[14−17] one might predict, therefore, that the reaction probability $P_{DCl+D\leftarrow Cl+D_2(\nu = 0)}$ of reaction 2 should be much smaller than $P_{HCl+H\leftarrow Cl+H_2(\nu = 0)}$ for reaction 1, for "only UV" experiments with the same laser parameters. Below we shall discuss, however, two additional, antagonistic effects for the reactions 3 in the quantum solids, rendering the conclusions less straightforward than for the gas phase.

The three isotope effects (i)−(iii) may be called energetic, because they are related to the isotope effects (8) and (15) as well as (10), (13), and (52) for the vibrational energies of the reactants and products and the correlated, nearly iso-energetic resonances and for their densities, respectively. These effects should be similar for the gas[14−17] and for the quantum solids, due to the rather weak interactions of the reactive systems with the surrounding quantum solids.

Second, we consider isotope effects that are specific for reactions 3 in the quantum solids initiated by "UV only" versus "IR + UV" experiments,[3] due to the isotope effects (23) and (31) for the translational energies and their widths, depending on the frequency ω of the UV laser. As discussed in section II, the width of the translational energy ΔE_{trans}^X increases with mass $2M_X$ of the molecules X_2 of the quantum crystals, because the width parameter Δx_{Cl+X_2} for the translational motions of the reactants is approximately equal to the widths partameter ΔR_{X_2} for the distributions of the molecular reactants in their Einstein cells, and this decreases with mass M_X; cf. eqs 16, 17, 27, and 28.[39] The trend may be extrapolated, on one hand, to the gas phase. There the width parameter for the distribution of the molecular reactants is arbitrarily large, $\Delta x_{Cl+X_2} \rightarrow \infty$, so that the widths of the translational energies approaches zero, $\Delta E_{trans}^X \rightarrow 0$. On the other hand, the trend may also be extrapolated to classical crystals with much larger masses of the molecular or atomic constituents, e.g., rare gas matrices. Here the translational motions of the particles are confined to rather small amplitudes, compared to those of the quantum solids.[39] As a consequence, the width of translational energies of laser induced reactions in classical crystals[10−12] is much larger than in quantum crystals. As a summary, the widths of the translational energies of the reactions in quantum solids ΔE_{trans}^X is between the limits of extremely small and large values for reactions in gases and in classical crystals, respectively. It is thus a challenge to investigate the general consequences of increasing values of ΔE_{trans}^X, or the corresponding decreases of the width parameters Δx_{Cl+X_2} of the wave functions of the reactants Cl + X_2, eqs 21 and 28−31, and to discover the corresponding isotope effects for the reactions 1 and 2 in quantum solids, in the context of the general trend from the gas to the classical solid. As a working hypothesis, the case of reaction 1 for the lighter para-H_2 with the smaller value of ΔE_{trans}^H should exhibit phenomena that remind us of the reactions in the gas phase, whereas reaction 2 for the heavier ortho-D_2 and larger ΔE_{trans}^D should show the opposite trend toward reactions in classical solids.

The effects of decreasing values of the widths parameters Δx_{Cl+X_2} and corresponding increasing values of ΔE_{trans}^X, eqs 28−34, are documented in Figures 3 and 4, for reactions 2 and 1, respectively. One readily notices several phenomena: (a) decreasing values of the width parameter Δx_{Cl+X_2} cause broadening and washing-out of the zigzag behaviors of the reaction probabilities versus total, i.e., translational (E_{trans}) plus vibrational ($\Delta E_{0\nu}^{XS}$) energies (34) of the reactants X_2 + Cl(ν), close to resonance energies. (b) The increase of the reaction probabilities

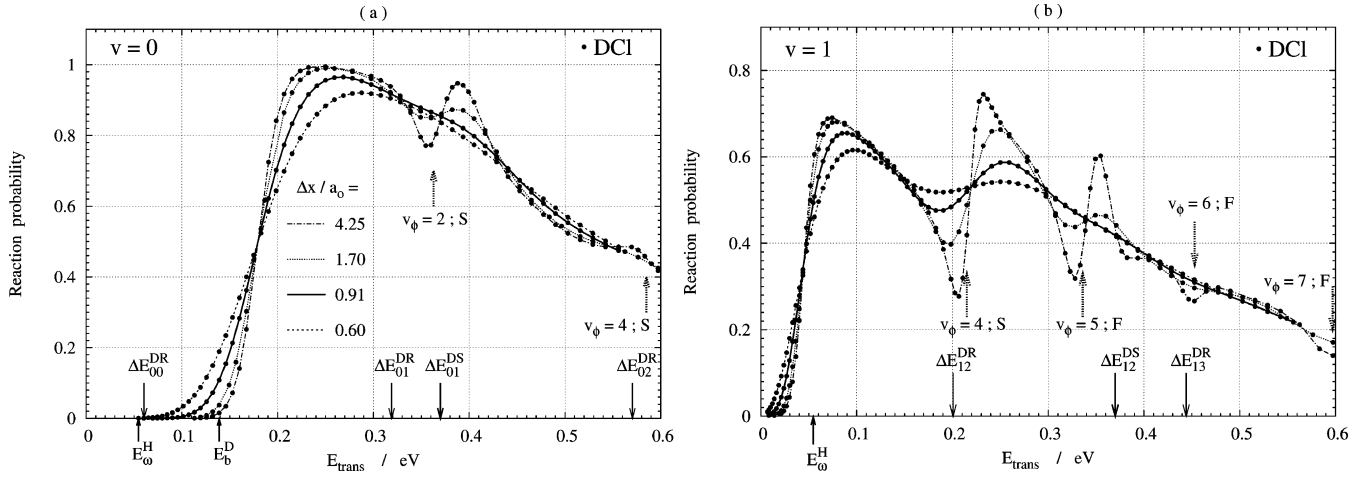

Figure 3. Reaction probabilities versus translational energies E_{trans} for the model $Cl + D_2(\nu) \rightarrow DCl + D$ reaction in solid ortho-D_2, depending on the width $\Delta x \equiv \Delta x_{Cl+D_2}$. Panels a and b show the results for $\nu = 0$ and 1, respectively. The solid lines are for the value $\Delta x_{Cl+D_2} = 0.90\ a_0$, which has been estimated from the distributions of the ortho-D_2 molecule and the precursor Cl_2 in their Einstein cells, eqs 18 and 26. Also indicated are the translational energy $E_\omega^D \equiv E_{\text{trans}}^D(\omega)$ for the UV frequency ω ($\lambda = 327.8$ nm) of the experiment,[3] the effective barrier E_b^D, eq 53, and the vibrational thresholds $\Delta_{\nu\nu'}^{DS}$ and $\Delta_{\nu\nu'}^{DR}$ for inelastic scattering and state-to-state reaction, eqs 48−51, together with the energies of the correlated resonances labeled ν_ϕ; compare with Figure 1.

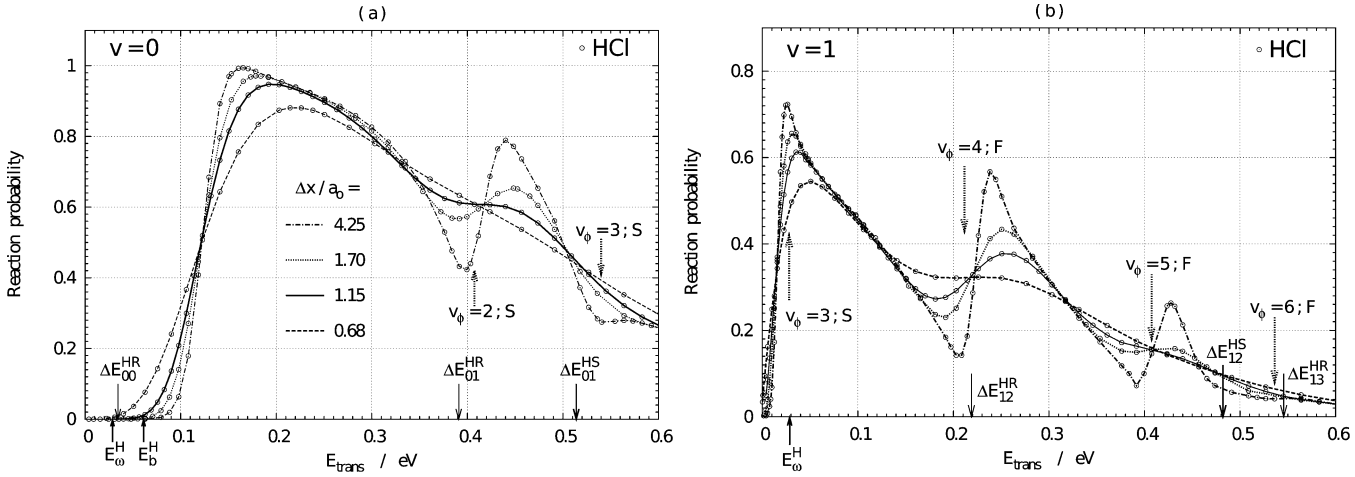

Figure 4. Same as Figure 3 but for the model $Cl + H_2(\nu) \rightarrow HCl + H$ reaction in solid para-H_2. The solid lines are for $\Delta x_{Cl+H_2} = 1.15\ a_0$.

from zero for $E_{\text{trans}} = 0$ to the first maximum value for $E_{\text{trans}} > 0$ changes systematically from sudden to smooth, as Δx_{Cl+X_2} decreases. These effects have been noticed first for the vibrationally state-selective $Cl + H_2(\nu)$ reactions 1 in ref 13, and they are confirmed here, also for the $Cl + D_2(\nu)$ reaction 2. They can be rationalized as follows:[13] For the reference case of reactions 3 in the gas, with energetic widths $\Delta E_{\text{trans}}^X$ close to zero, the reaction probabilities show sharp peaks or zigzag structures, as well as sudden increases to the first maximum.[15−17] For larger width $\Delta E_{\text{trans}}^X$, and corresponding smaller values of Δx_{Cl+X_2}, the wave functions $\Psi_{Cl+X_2(\nu),k_{Cl+X_2},\Delta x_{Cl+X_2}}(x,y,t)$ with mean translational energy E_{trans}^X and translational width $\Delta E_{\text{trans}}^X$ (30) may be written as superpositions of gas phase type partial waves $\tilde{\Psi}_{Cl+X_2(\nu),\tilde{k}_{Cl+X_2},\Delta\tilde{x}_{Cl+X_2}}(x,y,t)$ with narrow widths $\Delta\tilde{E}_{\text{trans}}^X$, and with momenta $\hbar\tilde{k}_{Cl+X_2}$ and corresponding translational energies $\tilde{E}_{\text{trans}}^X$, in the domain of the translational width $\Delta E_{\text{trans}}^X$; cf. ref 86. As a consequence, the wave functions $\Psi_{Cl+X_2(\nu),k_{Cl+X_2},\Delta x_{Cl+X_2}}(x,y,t)$ for the model reactions 3 in the quantum solids comprise some characteristic properties of the corresponding wave functions $\tilde{\Psi}_{Cl+X_2(\nu),\tilde{k}_{Cl+X_2},\Delta x_{Cl+X_2}}(x,y,t)$ for the reactions 3 in the gas phase covering, however, the broad range $\Delta E_{\text{trans}}^X$ of translational energies. Ultimately, this is imposed by the translational widths of the distributions of the molecules X_2 in the quantum solids, eqs 17, 18, and 27−30. For example, if the mean energy of $\Psi_{Cl+X_2(\nu),k_{Cl+X_2},\Delta x_{Cl+X_2}}(x,y,t)$ is centered within the width Γ_{ν_ϕ,ν_r} (44) of the resonance energy for the reaction in the gas phase, then the energetic wings of $\Psi_{Cl+X_2(\nu),k_{Cl+X_2},\Delta x_{Cl+X_2}}(x,y,t)$ may still penetrate into off-resonant domains, so that resonance peaks or zigzag features of the reactions 3 in the gas are reduced in the quantum solids. Likewise, even if the mean energy of $\Psi_{Cl+X_2(\nu),k_{Cl+X_2},\Delta x_{Cl+X_2}}(x,y,t)$ for the reaction probabilities in the quantum solids is out of the domain Γ_{ν_ϕ,ν_r} of reactions 3 in the gas, its energetic wings may penetrate into that domain; as a consequence, features of the resonance in the gas phase such as peaks or zigzag behaviors of the reaction probabilities may already appear in the quantum solid even if the mean energy is off-resonant with respect to the gas phase reference. The net effect is that the resonance energy domains of reactions 3 in the quantum solids cover and exceed the domains Γ_{ν_ϕ,ν_r} (44) of the reactions 3 in the gas. In brief: resonance phenomena of reactions 3 in the gas phase[15−17] are washed out and broadened in the quantum solids.

The analysis of the role of the translational width E_{trans}^X and the corresponding spatial width parameter Δx_{Cl+X_2} allows additional conclusions; for example, the resonance energy domains of all reactions 3 should overlap (namely, at least close to the domain Γ_{ν_ϕ,ν_r} (44) of the gas phase reference). This conjecture is confirmed by the overlapping domains of the

horizontal arrows that indicate the resonance energy domains of reaction 2; cf. Figure 1. Moreover, the increase of ΔE^{X}_{trans} with energy E^{X}_{trans}, eq 30, implies that the apparent resonance energy domains of reactions 3 in solids should also increase with translational energy. Again, this is confirmed by the results shown in Figure 1, in two ways: First, for a given mean total energy $E_{tot,Cl+X_2(\nu)}$ of the resonance, eq 36, the resonance energy domain increases with increasing values of E_{trans}, or with decreasing values of the vibrational energy $\Delta E^{DS}_{0\nu}$ for the vibrational quantum number ν. Second, for a given value of ν, the reaction probability may show significant features of the resonances at low values of E^{X}_{trans}, but these features are diminished, and they may even disappear for increasing values of E_{trans}. This wash-out effect may be supported by the fact that the resonance energy domains of neighboring resonances may overlap in the quantum solids, at higher translational energies, even if the corresponding resonances are energetically isolated in the gas. An intriguing example is the expected resonance that has been marked by a question mark, 6?;F, in Figure 2. Close inspection shows that its resonance energy domain overlaps with the rather broad domain for the neighboring resonance labeled 5;F. Apparently, the underlying resonance lifetime $\tau_{\nu_\phi=5,\nu_r}=0$ is longer than $\tau_{\nu_\phi=6,\nu_r}=0$, so that long time propagations of the wave functions (46) invariably yield the resonance wave function labeled $\nu_\phi = 5$ as the only survivor in the interaction domain, even if the mean total energy is close to the expected value for the resonance labeled $\nu_\phi = 6$. This special case calls for the development of extended methods, beyond those that have been applied here, based on ref 40.

Analogous arguments explain the broadening of the rise of the reaction probabilities from zero at $E^{X}_{trans} = 0$ to the first maximum at $E^{X}_{trans} > 0$: if it is sudden in the gas phase, then it will be broadened in the solid. A special case of this effect is noted if the sudden increase of the reaction probability occurs close to the reaction threshold, and if in addition there is a shape resonance close to the reaction threshold: The increase of the reaction probability versus E^{X}_{trans} may change from convex (zero or near zero derivative at $E^{X}_{trans} = 0$) to concave behavior (infinite or near infinite derivative at $E^{X}_{trans} = 0$), if the translational widths increases from small values below the gap between the mean resonance energy and the threshold to larger ones. A prominent example is shown for the case of the reaction $Cl + H_2(\nu = 1)$ close to the reaction threshold; see Figure 4b.

These effects of broadening and wash-out of resonance phenomena as well as the increases of reaction probabilities of reactions 3 in quantum solids increase with increasing values of ΔE^{X}_{trans}, which in turn increase with mass $2M_X$ of the X_2 molecule of the quantum solid. When these general trends are applied to the results for the specific larger and smaller values $\Delta x_{Cl+H_2} = 1.15\ a_0$[13] and $\Delta x_{Cl+D_2} = 0.90\ a_0$ for the $Cl + H_2(\nu)$ and $Cl + D_2(\nu)$ reactions, eqs 27−30, we discover the following isotope effects; see the continuous lines in Figures 3 and 4.

(iv) For the special cases of reactions 3 in the quantum solids, which may be induced by the "UV only" experiments or by IR + UV co-irradiation with sufficiently long durations $\tau \gtrsim 50$ fs (including the cases of nanosecond laser pulses or continuous wave (cw) excitations[3]), the rather broad translational distributions of the molecules in their Einstein cells (17) and (18)[39] impose the narrower spatial width parameter $\Delta x_{Cl+D_2} = 0.90\ a_0$ for reaction 2, compared to the broader parameter $\Delta x_{Cl+H_2} = 1.15\ a_0$ for reaction 1 (or 1.27 a_0, as estimated in ref 13); see eq 25. As a consequence implied by the preceding general analysis, the corresponding reaction probabilities versus E_{trans} yield broader and less pronounced zigzag type signatures of resonances for reaction 2 compared to those for reaction 1; cf. Figures 3 and 4, respectively. A prominent example is demonstrated for the resonance labeled $\nu_\phi = 2$: the zigzag signature is weak but clearly visible for $Cl + H_2(\nu = 0)$ (Figure 4a), whereas it has disappeared for $Cl + D_2(\nu = 0)$ (Figure 3a). This isotope effect puts reactions 3 in the quantum solids into the center between the limits of reactions in the gas phase, and in classical solids. More specifically, the larger and smaller translational amplitudes of the lighter $H_2(\nu)$ and the heavier $D_2(\nu)$ in their Einstein cells put reactions 1 and 2 in quantum solids closer to reactions in gas phase and in classical crystals, respectively.

(v) The slopes of the initial increases of the reaction probabilities from 0 for $E_{trans} = 0$ to the first maximum for $E_{trans} > 0$ are systematically steeper for reaction 1 in solid para-H_2 than for reaction 2 in solid ortho-D_2. Again, this puts reactions 3 into the center between the limits of reactions in the gas and in classical solids, with reactions 1 and 2 closer to the references of the gas and the classical solid, respectively. A prominent example is provided by the reactions $Cl + H_2(\nu = 0)$ in para-H_2 and $Cl + D_2(\nu = 0)$ in ortho-D_2, which may be induced by the "only UV" experiment.[3] For reference, significant product yields of the corresponding reactions 1 and 2 in the gas require translational energy E^{X}_{trans} slightly above the potential barrier E_b, specifically $E_{trans} \geq 0.18$ eV and 0.13 eV; see the crossing points of all reaction probabilities versus translational energy (irrespective of the width parameters Δx_{Cl+H_2} and Δx_{Cl+D_2}) that are shown in Figures 4a and 3a, respectively. For large values of Δx_{Cl+X_2}, corresponding to the gas phase reference, the slopes are steep,[15−17] whereas they decrease systematically for decreasing values of Δx_{Cl+X_2}. To summarize, the narrower translational amplitude of the heavier $D_2(\nu = 0)$ in its Einstein cell, compared to that for $H_2(\nu = 0)$, causes the smaller value $\Delta x_{Cl+D_2} = 0.90\ a_0$ compared to $\Delta x_{Cl+H_2} = 1.15\ a_0$ (or 1.27 a_0[13]), and this implies that the slope of the reaction probability versus E^{X}_{trans} is significantly smaller for the $Cl + D_2(\nu = 0)$ reaction in ortho-D_2 (1) than for the $Cl + H_2(\nu = 0)$ reaction 2 in para-H_2. As a consequence, for translational energies $E_{trans} < E^{X}_{b}$ below the barriers E^{X}_{b}, i.e., in the tunneling regime, the high energetic wings of the wave function $\Psi_{Cl+D_2,k_{Cl+D_2},\Delta x_{Cl+D_2}}(x,y,t)$ with broad translational energy width ΔE^{D}_{trans} may overcome the barrier, thus supporting reactivity, whereas the narrower ΔE^{H}_{trans} does not permit us to overcome the barrier, thus failing to support reactivity. This isotope effect (iv) implies that in the tunneling domain, reaction 2 should be more efficiently enhanced by its rather small spatial width Δx_{Cl+D_2}, compared to reaction 1. This is the first antagonistic isotope effect that has been anticipated at the end of the discussion of the energetic isotope effect (iii); obviously, it is an effect that occurs exclusively in solids, not in the gas. In fact, it is somewhat counterintuitive because it predicts the opposite trend (compared to the effect (iii)), i.e., enhanced reactivity of the heavier system in the tunneling domain.

Both isotope effects (iv) and (v) are consequences of the larger translational amplitudes of the lighter isotopomer $H_2(\nu)$ in its Einstein cell, compared to the case for $D_2(\nu)$, eq 31; hence they will be called translational amplitude effects.

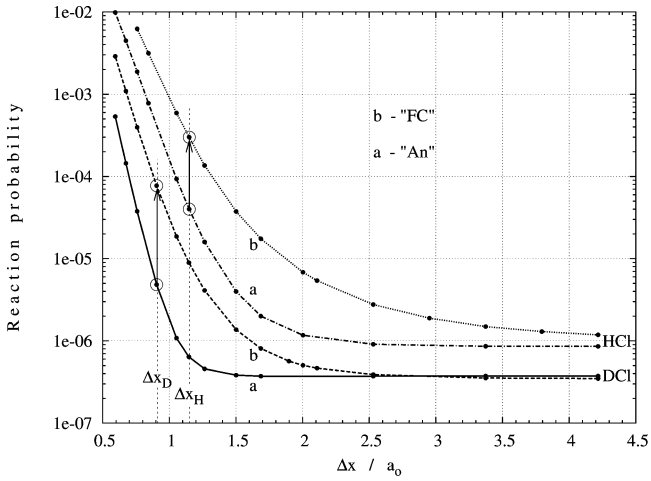

Figure 5. Comparison of the reaction probabilities $P_{XCl+X\leftarrow Cl+X_2(\nu),k(\omega),\Delta x}$ (eq 39, logarithmic plot) versus translational spatial width $\Delta x = \Delta x_{Cl+X_2}(\tau,\Delta R_{Cl_2},\Delta R_{X_2})$ (eqs 24−28) for the $Cl + H_2(\nu = 0) \rightarrow HCl + H$ reaction in solid para-H_2 (1) and the $Cl + D_2(\nu = 0) \rightarrow DCl + H$ reaction in solid ortho-D_2 (2), depending on the frequency ω of the "UV only" experiment. The curves labeled a and b are for the frequencies ω(An) and ω(FC) of the experiment of the group of Anderson[3] ($\lambda = 355$ nm) and for the resonant Franck−Condon transition to the excited $C^1\Pi_u$ state of the precursor Cl_2 molecule ($\lambda = 327.8$ nm). Changing ω(An) to ω(FC) induces different enhancements of the reactivities for reactions 1 and 2, as indicated by vertical arrows which are located at the corresponding widths labeled $\Delta x_H \equiv \Delta x_{Cl+H_2}$ and $\Delta x_D \equiv \Delta x_{Cl+D_2}$, respectively, assuming laser pulse durations $\tau > 50$ fs, cf. eqs 22−26. See text for discussion.

(vi) The second antagonistic isotope effect for reactions 3 in quantum solids, with the opposite trend compared to that in (iii), is a consequence of the kinetic isotope effect (23), i.e., for the given frequency ω of the UV laser in the "only UV" or "IR + UV" experiments, the resulting translational energy $E^X_{trans}(\omega)$ of the reactants $Cl + D_2(\nu)$ is about twice as large as for $Cl + H_2(\nu)$. For the experiment of the group of Anderson,[3] the UV photodissociation frequency ω is chosen below the resonance frequency for Franck−Condon excitation of the repulsive $C^1\Pi_u$ state of the precursor Cl_2 molecule. The resulting values of $E^D_{trans}(\omega)$ and $E^H_{trans}(\omega)$ are shown in Figures 3 and 4, respectively. They are well below the effective barriers E^X_b of the $Cl + X_2(\nu = 0)$ reactions, i.e., in the tunneling regime. As a rule, increasing translational energies support tunneling. The larger value of $E^D_{trans}(\omega)$ compared to $E^H_{trans}(\omega)$ enhances, therefore, the reaction probability of reaction 2 in solid ortho-D_2 more than reaction 1 in solid para-H_2. Hence, as for (v), the trend for the reactivity due to isotope effect (vi) is opposite to (iii).

The antagonistic isotope effects (iii) versus (v) and (vi), which diminish and enhance, respectively, the reactivity of the heavier reactants $Cl + D_2(\nu = 0)$ compared to those for $Cl + H_2(\nu = 0)$, make it rather difficult to make even just qualitative predictions about the net results and the trends depending on the experimental parameters, in particular the UV frequency ω. Quantitative predictions must rely on accurate quantum dynamics simulations. For the present model, we have investigated, in particular, the effects of increasing UV frequencies. Figure 5 shows the results (logarithmic plot) for the reaction probabilities $P_{XCl+X\leftarrow Cl+X_2(\nu),k(\omega),\Delta x}$ of reactions 3 versus the translational spatial width $\Delta x = \Delta x_{Cl+X_2}(\tau,\Delta R_{Cl_2},\Delta R_{X_2})$, eqs 24−28, for sufficiently long laser pulse durations, $\tau > 50$ fs, and for two different UV frequencies. One of them is labeled "An" for the Anderson experiment,[3] the other one "FC" for resonant Franck−Condon transition to the excited $C^1\Pi_u$ state of the precursor Cl_2 molecule. Obviously, for the given isotopomer and UV frequency, decreasing values of Δx imply increasing values of E^X_{trans} and, therefore, increasing values of reaction probabilities in the tunneling domain. Increasing the UV frequencies from ω(An) (λ(An) = 355 nm) to ω(FC) (λ(FC) = 327.8 nm) impies increasing values of translational energies $E^X_{trans}(\omega)$, eqs 20 and 22, supporting the reactivity even more. All these trends can be explained easily; see the preceding discussion. What is difficult or impossible to predict even qualitatively is the net result of the isotope effects (iii), (v), and (vi), i.e., whether the overall enhancement of the reactivity for reaction 1 is larger or smaller than that for reaction 2. For the present model, the quantitative result is shown in Figure 5. Apparently, increasing the UV frequency from ω(An) to ω(FC) will enhance the reaction probability of the reaction 1 from 0.4×10^{-4} by a factor of 7.5 to 0.3×10^{-3}. For reaction 2, the relative increase will be even larger, from 0.5×10^{-5} by a factor of 16 to 0.8×10^{-4}. At the same time, Figures 3b and 4b show that the effects of changing the UV frequency from ω(An) to ω(FC) will be rather modest, with factors close to 1, for both reactions 3. As a consequence of the different enhancement factors listed above, we predict that the ratio of reaction probabilities for the "UV + IR" experiment compared to that for the "UV only" experiments should have different, rather large, sensitivities with respect to the isotopomers, depending on the UV frequencies.

V. Conclusions

The results and analyses of the present quantum model simulations of reactions 1 and 2 in quantum solids para-H_2 and ortho-D_2 predict six isotope effects (i)−(vi). The discoveries for this prototype set of isotopomeric reactions, which has been well studied previously in the gas phase,[14−17] should be considered as examples. It is easy to predict similar isotope effects for analogous reactions in quantum solids, e.g., $Br + H_2(\nu) \rightarrow HBr + H$ in para-H_2 versus $Br + D_2(\nu) \rightarrow DBr + D$ in ortho-D_2, or $I + H_2(\nu) \rightarrow HI + H$ in para-H_2 versus $I + D_2(\nu) \rightarrow DI + D$ in ortho-D_2, etc.

In general, the isotope effects may be classified as energetic, translational amplitude, or kinematic effects. The present energetic effects (i), (ii), and (iii) are related to the vibrational thresholds and to the levels of correlated resonances. These should be similar to analogous energetic isotope effects of the reactions in the gas phase,[14−17] due to the rather weak interactions of the reactants with the quantum solids. In contrast, the large amplitude effects (iv) and (v) are due to the large amplitude translational motions of the molecules in Einstein cells of the quantum solids;[39]these are specific effects of reactions in quantum solids, which do not occur, neither in the gas phase nor in classical solids. The kinematic isotope effect (vi) should be present in quantum as well as in classical solids, and also in the gas phase.

In specific applications, several of the effects (i)−(vi) may contribute simultaneously, so that the net effects are characteristic for quantum solids if they involve effects (iv) and (v), possibly combined with others. For example, the kinematic effect (vi) puts the translational energy of the reactants $Cl + H_2(\nu = 0)$ and $Cl + D_2(\nu = 0)$ into the tunneling domain. Here the effects (iii) versus (iv) and (v) are antagonistic, which means reactivity is hindered or supported, respectively, by increasing the masses of the isotopomeric reactants. The interplay of isotope effects with opposite trends tends to make it difficult

TABLE 2: Vibrational Thresholds for Reactions[a]

v	v'	$\Delta E_{vv'}^{RD}$/eV	$\Delta E_{vv'}^{RH}$/eV
0	0	0.061	0.034
0	1	0.319	0.391
0	2	0.571	0.733
0	3	0.814	1.059
0	4	1.050	1.371
0	5	1.278	1.668
1	2	0.201	0.219
1	3	0.444	0.546
1	4	0.680	0.858
2	3	0.090	0.063
2	4	0.326	0.375
3	4	−0.013	−0.076

[a] Eqs 49 and 51.

or even impossible to anticipate the resulting variations of the ratio of the reaction probabilities for reaction 1 versus reaction 2, even qualitatively; see the discussion of the results shown in Figure 5. Quantitative predictions must rely on adequate quantum model simulations.

The analysis of isotope effects (iv) and (v) puts reactions 3 in quantum solids into the center between two extreme references: on one hand reactions in the gas phase; on the other hand reactions in classical solids. In particular, any signatures of reaction resonances, as well as sudden increases of reaction probabilities near the reaction thresholds or reaction barriers, which are prominent in the gas phase, disappear in classical solids. Reactions in quantum solids may still exhibit some of these phenomena, albeit in a broadened and partially washed-out manner. The systematic decrease of the amplitudes of translational motions, from quasi infinite in the gas phase to still quite large for the lighter isotopomer and somewhat smaller for the heavier one, until very small amplitudes of translational motions in classical solids, implies corresponding systematic trends of the isotope effects. In brief, the phenomena for reactions 1 and 2 tend to be more similar to those for the gas phase and the classical solid, respectively.

Throughout the discussion of the results, we have pointed to various net effects that should stimulate corresponding experiments. For example, the interplay of isotope effects (iii), (iv), (v), and (vi), which has been summarized above, implies that if one increases the UV frequency from the experimental value[3] to the one for resonant photodissociation of the precursor Cl_2 in the $C^1\Pi_u$ state, then the ratio of the reaction probabilities for the "only UV" versus "IR + UV" experiments should decrease more rapidly for the reaction of the heavier isotopers, $Cl + D_2(v)$, compared to the probability ratios of the lighter ones, $Cl + H_2(v)$; see the discussion of Figure 5. Likewise, using isotope effect (ii) we predict that the analogous IR + UV experiments for the reactions $Cl + H_2(v = 1) \rightarrow HCl + H$ (1) and $Cl + D_2(v = 1) \rightarrow DCl + D$ (2) should be qualitiatively different in the sense that (1) is supported by a shape resonance (see also ref 13), whereas (2) is not. As a consequence, extended time-dependent pump−probe experiments should discover different error-function type versus three-step-type formations of the products DCl + D versus HCl + H, respectively. In view of the simplicity of the model developed in ref 13, one should not expect that the present predictions are quantitative, but in any case, they should provide some guidance to experimental discoveries of isotope effects of reactions in quantum solids, a field that still appears as white territory on the landscape of reaction dynamics, compared to isotope effects of reactions in the gas phase.[46]

Acknowledgment. This paper is dedicated to Dr. Reinhard Schinke (Göttingen), in recognition of his pioneering contributions to quantum reaction dynamics.[46] We thank Prof. D. T. Anderson (Laramie) for stimulating discussions of his experiments[1–3] and Prof. M. Baer (Jerusalem) for pointing to his pioneering results for the $Cl + X_2$ reaction in the gas phase.[15–17] Financial support by the Deutsche Forschungsgemeinschaft (project Sfb 450 TP C1) and continuous support by Fonds der chemischen Industrie are also gratefully acknowledged.

References and Notes

(1) Raston, P. L.; Anderson, D. T. *Phys. Chem. Chem. Phys.* **2006**, *8*, 3124.
(2) Yoshioka, K.; Raston, P. L.; Anderson, D. T. *Int. Rev. Phys. Chem.* **2006**, *25*, 469.
(3) Kettwich, S. C.; Raston, P. L.; Anderson, D. T. *J. Phys. Chem. A* **2009**, *113*, 7621.
(4) Momose, T.; Fushitani, M.; Hoshina, H. *Int. Rev. Phys. Chem.* **2005**, *24*, 533.
(5) Yoshioka, K.; Anderson, D. T. *J. Chem. Phys.* **2003**, *119*, 4731.
(6) Fajardo, M. E.; Tam, S.; DeRose, M. E. *J. Mol. Struct.* **2004**, *695*, 111.
(7) Lundell, J.; Cohen, A.; Gerber, R. B. *J. Phys. Chem. A* **2002**, *106*, 11950.
(8) Khriachtchev, L.; Tanskanen, H.; Lundell, J.; Pettersson, M.; Kiljunen, H.; Räsänen, M. *J. Am. Chem. Soc.* **2003**, *125*, 4696.
(9) Feldman, V. I.; Sukhov, F. F.; Orlov, A. Y.; Tyulpina, I. V. *J. Am. Chem. Soc.* **2003**, *125*, 4698.
(10) Gerber, R. B. *Annu. Rev. Phys. Chem.* **2004**, *55*, 55.
(11) Khriachtchev, L.; Tanskanen, H.; Cohen, A.; Gerber, R. B.; Lundell, J.; Pettersson, M.; Kiljunen, H.; Räsänen, M. *J. Am. Chem. Soc.* **2003**, *125*, 6876.
(12) Khriachtchev, L.; Isokoski, K.; Cohen, A.; Räsänen, M.; Gerber, R. B. *J. Am. Chem. Soc.* **2008**, *130*, 6114.
(13) Korolkov, M. V.; Manz, J.; Schild, A. *J. Phys. Chem. A* **2009**, *113*, 7630.
(14) Persky, A.; Klein, F. S. *J. Chem. Phys.* **1966**, *44*, 3617.
(15) Baer, M. *Mol. Phys.* **1974**, *27*, 1429.
(16) Persky, A.; Baer, M. J. *J. Chem. Phys.* **1974**, *60*, 133.
(17) Baer, M.; Halavee, U.; Persky, A. *J. Chem. Phys.* **1974**, *61*, 5122.
(18) Skouteris, D.; Manolopuolos, D. E.; Bian, W.; Werner, H.-J.; Lai, L.-H.; Liu, K. *Science* **1999**, *286*, 1713.
(19) Capecchi, G.; Werner, H. J. *Chem. Phys. Phys. Chem.* **2004**, *6*, 4975.
(20) Skouteris, D.; Laganá, A.; Capecchi, G.; Werner, H.-J. *Int. J. Quantum Chem.* **2004**, *99*, 577.
(21) Balucani, N.; Skouteris, D.; Capozza, G.; Segoloni, E.; Casavecchia, P.; Alexander, M. H.; Capecchi, G.; Werner, H.-J. *Phys. Chem. Chem. Phys.* **2004**, *6*, 5007.
(22) Mahapatra, S. *Int. Rev. Phys. Chem.* **2004**, *23*, 483.
(23) Wang, X.; Dong, W.; Xiao, C.; Che, L.; Ren, Z.; Dai, D.; Wang, X.; Casavecchia, P.; Yang, X.; Jiang, B.; Xie, D.; Sun, Z.; Lee, S.-Y.; Zhang, D. H.; Werner, H.-J.; Alexander, M. H. *Science* **2008**, *322*, 573.
(24) Connor, J. N. L.; Jakubetz, W.; Manz, J. *J. Chem. Phys.* **1978**, *28*, 219.
(25) Connor, J. N. L.; Jakubetz, W.; Manz, J.; Whitehead, J. C. *J. Chem. Phys.* **1980**, *72*, 6209.
(26) Connor, J. N. L.; Jakubetz, W.; Laganá, A.; Manz, J.; Whitehead, J. C. *Chem. Phys.* **1982**, *65*, 29.
(27) Bondi, D. K.; Connor, J. N. L.; Manz, J.; Römelt, J. *Mol. Phys.* **1983**, *50*, 467.
(28) Engel, V.; Schinke, R. *J. Chem. Phys.* **1988**, *88*, 6931.
(29) Hartke, B.; Manz, J. *J. Am. Chem. Soc.* **1988**, *110*, 3063.
(30) Hartke, B.; Manz, J. *J. Chem. Phys.* **1990**, *92*, 220.
(31) Manz, J.; Römelt, J. *J. Chem. Soc. Faraday Trans.* **1990**, *86*, 1689.
(32) Combariza, J. E.; Daniel, C.; Just, B.; Kades, E.; Kolba, E.; Manz, J.; Malisch, W.; Paramonov, G. K.; Warmuth, B. In *Isotope Effects in Gas Phase Chemistry*; Kaye, J. A., Ed.; ACS Symposium Series No. 502; American Chemical Society: Washington, DC, 1992; p 310.
(33) Mauersberger, K.; Krankowsky, D.; Janssen, C.; Schinke, R. *Adv. At. Mol. Opt. Phys.* **2005**, *50*, 1.
(34) Schinke, R.; Grebenshchikov, S. Y.; Ivanov, M. V.; Fleurat-Lessard, P. *Annu. Rev. Phys. Chem.* **2006**, *57*, 625.
(35) Kohen, A.; Limbach, H.-H. *Isotope Effects in Chemistry and Biology*: CRC Press: Boca Raton, FL, 2006.
(36) Sun, Z. G.; Liu, L.; Lin, S. Y.; Schinke, R.; Guo, H.; Zhang, D. H. *Proc. Natl. Acad. Sci. U.S.A.* **2010**, *107*, 555.
(37) Silvera, I. F. *Rev. Mod. Phys.* **1980**, *52*, 393.
(38) Operetto, F.; Pederiva, F. *Phys.Rev. B* **2006**, *73*, 184124.

(39) Kühn, O.; Manz, J.; Schild, A. *J. Phys.: Condens. Mattter* **2010**, *22*, 135401.
(40) Korolkov, M. V.; Manz, J. *Chem. Phys.* **2010**, *370*, 159.
(41) Manz, J. *J. Am. Chem. Soc.* **1980**, *102*, 1801.
(42) Connor, J. N. L.; Jakubetz, W.; Manz, J. *Mol. Phys.* **1978**, *35*, 1301.
(43) Apkarian, V. A.; Schwentner, N. *Chem. Rev.* **1999**, *99*, 1481.
(44) Korolkov, M. V.; Manz, J. In *Analysis and Control of Ultrafast Photoinduced Reactions*; Kühn, O., Wöste, L., Eds.; Springer Series in Chemical Physics No. 87; Springer: Berlin, 2007; Chapter 4.10, p 352.
(45) Bargheer, M.; Cohen, A.; Gerber, R. B.; Gühr, M.; Korolkov, M. V.; Manz, J.; Niv, M. Y.; Schröder, M.; Schwentner, N. *J. Phys. Chem. A* **2007**, *111*, 9573.
(46) Schinke, R. *Photodissociation Dynamics*; Series on Atomic and Molecular Physics; Cambridge University Press: Cambridge, New York; 1993.
(47) Eshet, E.; Ratner, M. A.; Gerber, R. B. *Chem. Phys. Lett.* **2006**, *431*, 199.
(48) Cohen, A.; Gerber, R. B. *Chem. Phys. Lett.* **2007**, *441*, 48.
(49) London, F. *Z. Elektrochem.* **1929**, *35*, 552.
(50) Eyring, H.; Polanyi, M. *Z. Phys. Chem. B* **1931**, *12*, 279.
(51) Sato, S. *J. Chem. Phys.* **1955**, *23*, 592.
(52) Launay, J. M.; Dourneuf, M. Le. *J. Phys. B: At. Mol. Phys.* **1982**, *15*, L455.
(53) Neumark, D. M. *Acc. Chem. Res.* **1993**, *26*, 33.
(54) Qiu, M.; Ren, Z.; Che, L.; Dai, D.; Harich, S. A.; Wang, X.; Yang, X.; Xu, C.; Xie, D.; Gustafsson, M.; Skodje, R. T.; Sun, Z.; Zhang, D. H. *Science* **2006**, *311*, 1440.
(55) Kuppermann, A.; Kaye, J. A.; Dwyer, J. J. *Chem. Phys. Lett.* **1980**, *74*, 257.
(56) Hauke, G.; Manz, J.; Römelt, J. *J. Chem. Phys.* **1980**, *73*, 5040.
(57) Manz, J.; Meyer, R.; Römelt, J. *Chem. Phys. Lett.* **1983**, *96*, 607.
(58) Manz, J.; Meyer, R.; Pollak, E.; Römelt, J. *Chem. Phys. Lett.* **1982**, *93*, 184.
(59) Manz, J.; Meyer, R.; Pollak, E.; Römelt, J.; Schor, H. H. R. *Chem. Phys.* **1984**, *83*, 333.
(60) Manz, J.; Schor, H. H. R. *Chem. Phys. Lett.* **1984**, *107*, 542.
(61) Kulander, K. C.; Manz, J.; Schor, H. H. R. *J. Chem. Phys.* **1985**, *82*, 3088.
(62) Bisseling, R. H.; Kosloff, R.; Manz, J. *J. Chem. Phys.* **1985**, *83*, 993.
(63) Manz, J.; Schor, H. H. R. *J. Phys. Chem.* **1986**, *90*, 2030.
(64) Bisseling, R. H.; Kosloff, R.; Manz, J.; Mrugała, F.; Römelt, J.; Weichselbaumer, G. *J. Chem. Phys.* **1987**, *86*, 2626.
(65) Gertitschke, P. L.; Kiprof, P.; Manz, J. *J. Chem. Phys.* **1987**, *87*, 941.
(66) Joseph, T.; Manz, J.; Mohan, V.; Schreier, H.-J. *Ber. Bunsen-Ges. Phys. Chem.* **1988**, *92*, 397.
(67) Karrlein, W.; Manz, J.; Mohan, V.; Schreier, H.-J.; Spindler, T. *Mol. Phys.* **1988**, *64*, 563.
(68) Kubach, C. *Chem. Phys. Lett.* **1989**, *164*, 475.
(69) Bisseling, R. H.; Gertitschke, P. L.; Kosloff, R.; Manz, J. *J. Chem. Phys.* **1989**, *88*, 6191.
(70) Hartke, B.; Manz, J.; Mathis, *J. Chem. Phys.* **1989**, *139*, 123.
(71) Nguyen Vien, G.; Richard-Viard, M.; Kubach, C. *J. Phys. Chem.* **1991**, *95*, 6067.
(72) Hartke, B.; Janza, A. E.; Karrlein, W.; Manz, J.; Mohan, V.; Schreier, H.-J. *J. Chem. Phys.* **1992**, *96*, 3569.
(73) Fischer, R. A.; Gertitschke, P. L.; Manz, J.; Schor, H. H. R. *Chem. Phys. Lett.* **1989**, *156*, 100.
(74) Joseph, T.; Kruel, T. M.; Manz, J.; Rexrodt, I. *Chem. Phys.* **1987**, *113*, 223.
(75) Manz, J.; Pollak, E.; Römelt, J. *Chem. Phys. Lett.* **1982**, *86*, 26.
(76) Pollak, E.; Wyatt, R. E. *J. Chem. Phys.* **1982**, *77*, 2689.
(77) Pollak, E. *J. Chem. Phys.* **1983**, *78*, 1228.
(78) Pollak, E.; Römelt, J. *J. Chem. Phys.* **1984**, *80*, 3613.
(79) Davis, M. J.; Stechel, E. B.; Heller, E. J. *Chem. Phys. Lett.* **1980**, *76*, 21.
(80) Heller, E. J.; Stechel, E. B.; Davis, M. J. *J. Chem. Phys.* **1980**, *73*, 4720.
(81) Briggs, J. S.; Kades, E.; Manz, J.; Rost, J. M.; Schlier, C.; Seiter, A. *Z. Phys. Chem.* **1996**, *195*, 65.
(82) Taylor, J. R. *Scattering Theory — The Quantum Theory of Nonrelativistic Collisions*; John Wiley & Sons: New York, 1972.
(83) Lee, Y. T. *Angew. Chem. Int. Ed. Engl.* **1987**, *26*, 939.
(84) Heller, E. J.; Manz, J. *Z. Phys. D: At. Mol. Clusters* **1989**, *13*, 281.
(85) Skodje, R. T.; Skouteris, D.; Manolopoulos, D. E.; Lee, S.-H.; Dong, F.; Liu, K. *Phys. Rev. Lett.* **2000**, *85*, 1206.
(86) Tannor, D. J. *Introduction to Quantum Mechanics — A Time-Dependent Perspective*; University Science Books: Sausalito, CA, 2007.

JP102809P